# Mapping of fracture corridors in the basement rocks of the Øygarden Complex, Western Norway

Master Thesis

Basin and Reservoir Studies

Eirin Hermansen


University of Bergen

Department of Earth Science

June, 2019

# ABSTRACT

Fracture corridors, defined as tabular zones of enhanced fracture intensity, are common features in both sedimentary and crystalline rocks. As potential high permeable structures, research has shown that fracture corridors have significant effect on fluid flow in subsurface reservoirs, e.g. by causing early water break through or compromise top seal integrity in hydrocarbon reservoirs. Yet, the mechanisms for their development, geometrical and fluid flow properties are poorly understood. With a growing interest in basement plays on the Norwegian continental shelf following the Rolvsnes hydrocarbon discovery, an improved knowledge of the intrinsic architecture of fracture corridors in basement rocks is valuable.

By detailed outcrop mapping and digitization of fracture patterns in fracture corridors in the basement rocks of the Øygarden Complex on Sotra, SW Norway, this study aims to broaden the knowledge of the spatial distribution of fractures and topological parameters within fracture corridors. The methodology combines a characterisation of the geometric properties (fracture orientations, abundance, distribution) with topology, which characterise the spatial relationship between fractures. This enabled both geometric and fluid flow properties, such as the connectivity, of different types of fracture corridors to be quantified.

Results show that the fracture intensity within fracture corridors are about three to six times higher than in the immediate surroundings. The fracture corridors mainly consist of sub-parallel fractures, resulting in a low to intermediate connectivity and an anisotropic flow direction. As the majority of fractures are not sealed by minerals of fault gouge, the abundance of fracture corridors observed onshore indicate that these features are significant also in the basement plays on the Norwegian Continental Shelf. This study has developed an extensive database of fracture attributes, which is utilized to investigate the spatial arrangement and possible models for the development of fracture corridors in the basement rocks on Sotra.

This study has documented and quantified geometric and topological parameters based on fracture patterns observed in outcrops, and as basement plays are poorly constrained by seismic data, the spatial arrangement of fracture corridors found through this study can improve the understanding of fluid flow in basement reservoirs on the NCS.

# ACKNOWLEDGEMENTS

Throughout this project I have received valuable support and assistance, and I would like to express my sincere gratitude to all of you who have contributed to this project.

First and foremost, I wish to thank my supervisor Eivind Bastesen at NORCE Research for his guidance, inspiration and feedback. I also wish to express my gratitude to the Department of Earth Science at the University of Bergen, and to the ANIGMA project from the Research council in Norway through the ENERGIX program for financial support. I would also like to thank Prof. David J. Sanderson and David Peacock for sharing their knowledge and data regarding fracture corridors in the Bergen area. For introducing me to Network GT and offering his help, I would like to thank Bjørn Burr Nyberg. To my fellow students Rebecca and Thea I express my appreciation for their assistance during fieldwork and constructive inputs that have improved my work. Finally, I wish to thank my family, friends and the girls at Hovedkvarteret who have all contributed in different and highly valued ways, and give a special thanks to my dad, Hroar, for his support, thorough reviews and inputs.

Eirin Hermansen

Bergen, June 2019

# TABLE OF CONTENT

# 1 INTRODUCTION

## 1.1 Rationale

The majority of fractures visible in outcrops are not the result of surface conditions, hence similar structures also occur in the subsurface (Nelson, 1985). Because of their potential as fluid conduits or baffles in hydrocarbon and geothermal reservoirs, faults and fractures have been the subjects of numerous studies (e.g. Caine et al., 1996; Wibberley et al., 2008). Fracture corridors (linear zones of enhanced fracture intensity), have, despite being common features in outcrops and potentially high permeable structures, received less attention and the basis for defining their characteristics and properties is insufficient.

Questiaux et al. (2010) demonstrated how incorporating fracture corridors in simulations of real-life oil fields increased the consistency between simulated outcome and the actual result. Hence, fracture corridors were interpreted as significant features in some reservoirs, and are therefore important to detect in order to construct proper models and predictions of the reservoir flow dynamics. Detecting fracture corridors by seismic imaging and borehole image logs has, however, been found to be challenging (Ozkaya and Richard, 2006; Questiaux et al., 2010). Thus, detailed outcrop studies of fracture corridors are valuable sources of information to acquire a proper understanding of similar features in the subsurface.

In tight rocks, such as crystalline basement rocks, porosity and permeability is controlled by fracture networks (Nelson, 2001). However, the majority of outcrop-based studies on fracture corridors have been focused on sedimentary rocks (e.g. Ogata et al., 2014; Souque et al., 2019). In recent years, the interest for fracture systems in tight rocks has increased due to increased amount of discoveries of hydrocarbon resources in basement reservoirs (Belalidi et al., 2016), and their propriety for geothermal energy (McNamara et al., 2014). Following the Rolvsnes oil discovery in fractured and weathered basement rocks (Riber et al., 2015), understanding the basement plays on the Norwegian continental shelf has become essential, and the basement rocks on Sotra could act as possible analogues.

Fracture corridors in basement have previously been studied by Gabrielsen and Braathen (2014). They identified a zonational fracture distribution within fracture corridors, and proposed a model for the development of fracture corridors based on observations in western Norway. Furthermore, mechanical and petrophysical properties (e.g. permeability, hardness of the rock, velocity) of fracture corridors in the basement complex on Sotra has been assessed by Torabi et al. (2018) and compared to the properties of a subsurface drill core from similar lithology just offshore Sotra. Various authors have addressed the lack of a quantitative basis for defining fracture corridors. Hence, the recent study by Sanderson and Peacock (2019) proposed a number of methods enabling a definition of and characterisation of the spatial variability of fractures in fracture corridors. However, more knowledge of geometry and spatial distribution of geometric properties, fracture intensity and connectivity within fracture corridors is needed to better understand how these structures might affect fluid flow in potential groundwater-, geothermal- and hydrocarbon reservoirs, which is the reason this study has been conducted.

## 1.2 Aims and Objectives

The primary aim of this study is to increase the knowledge of geometric and topological properties of fracture corridors; hence, contribute to a better understanding of how these fracture corridors might affect fluid flow in geothermal and hydrocarbon basement reservoirs. Following objectives outline how this study has been arranged in order to achieve this.

- Collect structural data from field outcrops and characterise the internal structure of a fracture corridor by assessing the fracture geometry, fracture intensity and distribution of fractures and geometric properties.
- Characterise the fracture network topology and investigate spatial distribution of topological properties so that an estimation of the connectivity of these fracture corridors can be made.

## 1.3 Study Area

West of Bergen on the island Sotra, the Precambrian basement complex, named the Øygarden Complex, is exposed, which provide excellent outcrops for field investigations of fractured basement rocks. The Øygarden Complex is positioned in the core of the characteristic Bergen Arc system that formed during the Caledonian orogeny (Wiest et al., 2018, and references therein). Furthermore, the Øygarden Complex is characterised by two conjugate lineament sets, trending NW-SE and NE-SW, that formed during multiphase extensional tectonics following the Caledonian Orogeny (Larsen et al., 2003). Further information about the geology of the study area is provided in chapter 3.

The focus of attention during this project has been fracture corridors along the western coast of Sotra. As access to fracture corridors is often limited by vegetation and topography, the locations on Sotra are unique as they are located close to the ocean, hence; non-vegetated, which has enabled a detailed study of fracture distribution across several fracture corridors.

**Figure 1.3-1 Example of fracture corridor from the Nesvika field location Photo: Eirin Hermansen**

# 2 CONCEPTS AND TERMINOLOGY

This projects objective is to contribute to a better understanding of the spatial distribution of fractures within fracture corridors and how fracture corridors might affect fluid flow in tight, crystalline rocks. Thus, this chapter will present some of the basic terminology associated with fracture corridors and basement reservoirs.

## 2.1 Brittle deformation

Brittle deformation is by Van der Pluijm and Marshak (2004) described as accumulation of permanent strain in a solid material, either by formation of or sliding on fractures following a critical differential stress. Fractures are among the most common features in the upper crust and of significant interest within different fields (Nelson, 1985). Fractures are defined following Fossen (2010) as a planar to sub-planar discontinuity, representing both a displacement- and mechanical discontinuity in the rock. Based on the sense of displacement fractures and fracturing is further subdivided into mode I (extension fractures), mode II (shear fractures and faults) and mode III (hybrid fractures) (Figure 2.1-1) (e.g. Schultz and Fossen, 2008; Fossen, 2010). Opening mode fractures are further subdivided into joints, fissures, veins and dikes, while mode II fracturing creates shear fractures and faults. Hybrid fractures develop by a combination of mode I and II deformation. Characteristics and their relation to

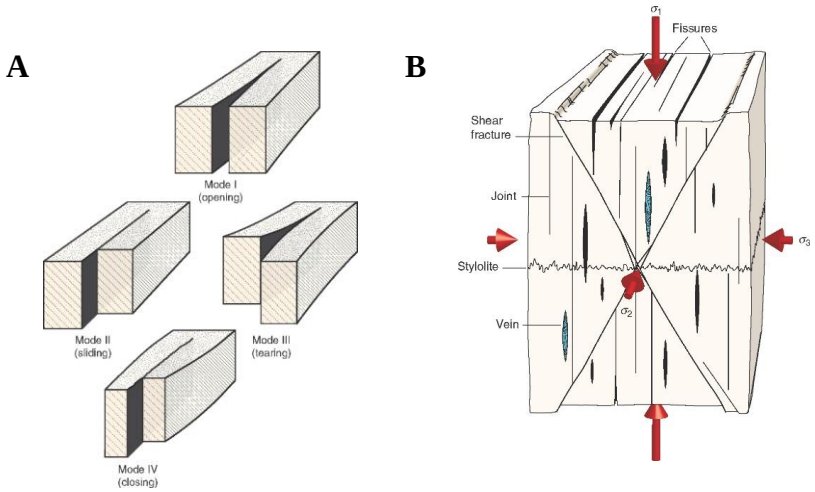


**Figure 2.1-1 A) The different fracturing modes B) Different fracture types and their relationship to the principal stress axes Fossen (2010)**

the principal stress axes are illustrated in Figure 2.1-1.

## 2.2 Fracture Corridors

A fracture network is characterised as a system of fractures within the same rock volume, and may consist of fractures of different sets (Berkowitz et al., 2000).

The main subject of this study; fracture corridors, are characterized as narrow, tabular zones with enhanced fracture frequency compared to the background (regional) fracture pattern (Gabrielsen & Braathen 2014). Fracture corridors commonly comprise continuous features, up to several kilometres long, although the trace lengths of the fractures within the corridor vary (e.g. Gabrielsen & Braathen, 2014; Ogata et al. 2014; Souque et al. 2019). Furthermore, it has been recommended that the term fracture corridor should be confined to cases of abrupt changes in fracture intensity and to swarms of mainly parallel to sub-parallel fractures, while more diffuse changes in intensity and heterogeneous fracture orientations are termed fracture swarms (Figure 2.2-1) (Sanderson and Peacock, 2019; Souque et al., 2019). Commonly, fracture corridors consist of mixed mode fractures (Gabrielsen and Braathen, 2014), and are often spatially associated with faults, forming the encompassing damage zone (Gabrielsen and Braathen, 2014; Ogata et al., 2014; Ozkaya, 2006; Souque et al., 2019). However, in cases where distinct fracture types comprise the majority of the fractures it is suggested that a more descriptive term is used, e.g. joint swarm (Gabrielsen & Braathen, 2014). Thus, most faults can be classified as fracture corridors, but not all fracture corridors are faults (Gabrielsen et al. 2002).

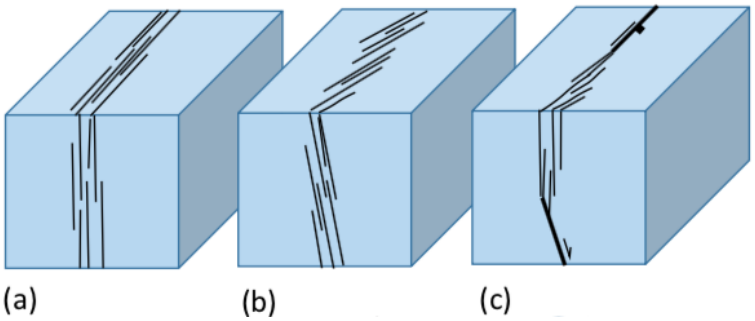


**Figure 2.2-1 Different types of fracture swarms a) fracture corridor b) fracture array or shear zone c) fault damage zone. Differentiated by fracture orientations. From Sanderson and Peacock (2019)**

Various models have been proposed for the mechanisms of fracture corridor formation (e.g. Braathen and Gabrielsen, 1998; Stephenson et al., 2007; Gabrielsen and Braathen, 2014; Ogata et al., 2014, Souque et al., 2019). Fold related fracture corridors are found in the Zagros Mountains, interpreted to form by flexural slip folding (Stephenson et al. 2007). Souque et al. (2019) found that fracture corridors in carbonate rocks were geometrically linked (connecting surfaces) to faults, and argued that the fracture corridors nucleated in areas of stress concentrations along a fault.

The study by Gabrielsen & Braathen (2014) suggested that joint swarms, fracture corridors and faults in basement rocks represent different stages of development and strain intensity. Thus, with increased deformation a joint swarm could develop into a fault. They based this interpretation on a zonational architecture (Figure 2.2-2), and proposed a model for classifying faults and fracture corridors based on geometry, spatial fracture pattern and distribution of fault rocks. Following this classification, the structure of faults and fracture corridors are subdivided into five zones (A-E), with a decreasing fracture frequency from the central part; zone A (synonymous to fault core), to the outer boundary; zone E. All subzones are not present at all times, reflecting different strain accumulation.

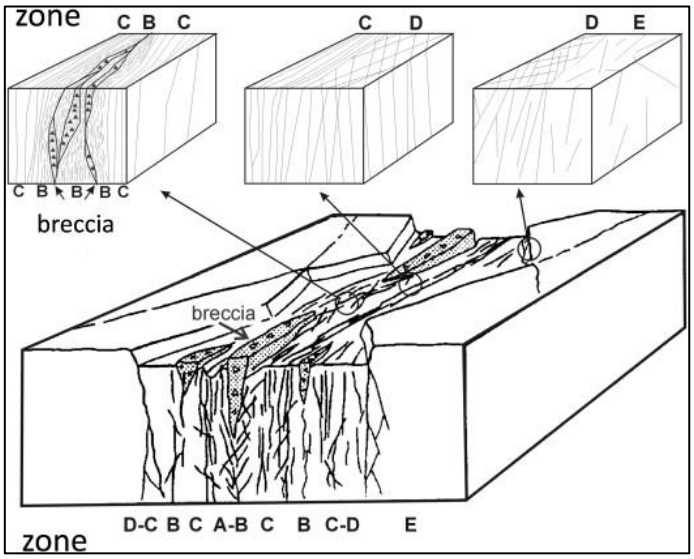


**Figure 2.2-2 The zonational architecture from the central sub-zones A-B to the boundary sub-zone E. As illustrated in not all sub-zones are present in all fracture corridors. From Gabrielsen and Braathen (2014).**

The inner area of a fracture corridor, zone A and B, is characterised by the highest fracture frequencies, various fracture orientations, fractures arranged in overlapping en echelon or cross-cutting patterns, secondary mineralizations, bleaching haloes, and may comprise

fracture planes with striated surfaces and fault rocks. Zone C comprise one or two fracture sets sub-parallel to the corridor, fracture orientations in zone D is less homogeneous. Secondary mineralizations and bleaching haloes seldom occur or is absent in both zones. Lozenge or diamond shaped rock fragments are separated by Mode I fractures, and often generate the steep valley sides of the fracture corridor. The outer boundary of a fracture corridor is marked by zone E, and Gabrielsen and Braathen (2014).

### 2.2.1 Fracture corridors as fluid flow conduits

Fractures affect the porosity and permeability of a rock volume by acting as conduits, baffles or barriers (e.g. Braathen and Gabrielsen, 1998). Depending on the composition of both the fluid and host rock, the fluid circulation may increase, or reduce the porosity and/or permeability by dissolution of minerals or fracture sealing by secondary mineralization (Gutmanis, 2009; Trice, 2014). Thus, the fracture geometry (e.g. orientation and trace length) and connectivity are important properties to characterise associated with production of hydrocarbons, geothermal energy and groundwater wells.

Based on the high fracture intensity fracture corridors are potential high permeable structures, and were by Ozkaya (2019) described as “permeability highways”. However, as shown by Gabrielsen and Braathen (2014) the fluid conductivity of fracture corridors in tight, crystalline rocks depend on various factors such as secondary mineralization, fault rock distribution and clay

In hydrocarbon reservoirs, there has been found evidence that water invasions into the reservoir and thief zones might be caused by the presence of fluid conductive fracture corridors (Ozkaya, 2019). The study by Questiaux et al. (2010) showed that including fracture corridors when simulating the fluid flow in hydrocarbon reservoirs, improved the correlation between the simulated outcome and the actual result. The significance of fractures within basement reservoirs is further explained in the following section.

## 2.3 Basement reservoirs

Although a variety of definitions exist, the term basement is generally applied when referring to igneous and metamorphic rocks that are unconformably overlain by a sedimentary cover (Koning, 2003). As basement rocks are often tight, crystalline rocks with little to no matrix porosity and permeability, basement reservoirs are classified as Type 1 reservoirs following

Nelson (2001). Thus, the fracture network controls the porosity and permeability of the reservoir. Characterising and understanding fracture networks within basement rocks is therefore fundamental to create proper models of the reservoir.

Fractured reservoirs are complex and challenging as they respond differently and comprise several variables that make reservoir behaviour difficult to predict (Nelson, 1985). Hence, fractured basement reservoirs have until recent years been underexplored despite examples of successful hydrocarbon production in eg. Yemen and Vietnam (Gutmanis, 2009; Trice 2014, and references therein) and the potential for storing and extracting geothermal energy as in New Zealand (McNamara et al., 2014). As of today, there are no producing basement reservoirs on the Norwegian continental shelf (NCS). However, following the oil discovery Rolvsnes within fractured and weathered basement rocks on the Utsira High, basement plays on the NCS are receiving more attention.

## 2.4 Topology

In tight and low permeable rocks, fracture networks are key conduits for fluid migration as the fractures control the porosity and permeability of the rock (Berkowitz et al., 2000). For a fracture network to facilitate fluid flow it is essential that the fractures are connected (Singhal and Gupta, 2010). Thus, it is important to characterise the geometric relationship between the fractures to assess how fluids may migrate through the fracture network. For this reason the concept of topology has been adapted to fracture network characterisation (Manzocchi, 2002; Singhal and Gupta, 2010; Sanderson and Nixon, 2015). Herein, an introduction of the terminology associated with topological analysis is presented, while a description of how topology has been applied in this project is further explained in chapter 4.

Geometric properties such as strike, frequency, size, aperture and spatial correlation are factors that affect the connectivity of a network (Peacock, 2016, and references herein). Characterising the topology is fundamental to assess the connectivity as fracture networks consisting of similar geometric elements may have critically different connectivity based on the spatial arrangement of fractures (Sanderson and Nixon, 2015).

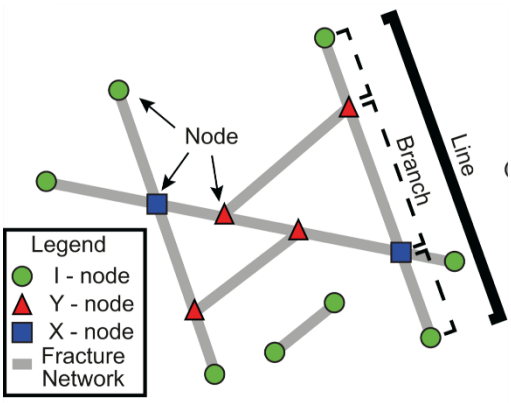


**Figure 2.4-1 Terminology related to topology. Fractures are explained by lines (the full length of the fracture), nodes (ends or intersection points) and branches (segment of a line bounded by two nodes). From Nyberg et al. (2018)**

Following Sanderson and Nixon (2015), to assess the topology fractures are described using lines, nodes and branches (Figure 2.4-1). A line is the full length of a fracture, and may consist of one or more branches, which in turn are segments of a line from one node to another. Thus, a branch is bounded a maximum of two nodes. Nodes are defined as ends- or intersection points of fractures. Three types of nodes are applied: isolated I-nodes and the connecting X- (crossing intersections) and Y-nodes (abutments and splays). This terminology is illustrated in Figure 2.4-1. Furthermore, the two nodes that bound a branch are used to classify the branch as either I-I, meaning the branch is bounded by two isolated nodes, I-C (isolated-connected) or C-C (connected – connected).

An estimation of the connectivity can be derived from the proportion of different types of nodes and branches. Fracture networks with higher proportions of connecting nodes and branches have greater connectivity as Y-nodes connects three branches and an X-node four (Sanderson and Nixon, 2015). A quantitative measure of the connectivity of the network can be derived based on the number of connections per branch ($C_B$), which is a number between 0 and 2. Furthermore, the connective properties of the network are often visualized by plotting the topological parameters in ternary diagrams and density maps.

# 3 GEOLOGICAL FRAMEWORK

## 3.1 The Øygarden Complex

The study area of this project is located within the exposed basement rocks of the Øygarden Complex (ØC) on the island Sotra. The Øygarden Complex is positioned in the centre of the Bergen Arc system, west of the allochthonous units that were thrusted onto the basement of the Baltic shield during the Caledonian orogeny (Figure 3.1-1) (Fossen and Rykkelid, 1990).

Despite a consensus on a Precambrian origin of the Øygarden Complex, a more precise age and evolution has for decades been a subject of debate (Sturt et al., 1975; Larsen et al., 2003; Wiest et al., 2018). However, U-Pb zircon geochronology presented by Wiest et al. (2018) confirmed a Precambrian age, and identified the Øygarden Complex as part of the Proterozoic Telemarkia (1,52-1,48 Ga) terrane. Based on the similar ages and position, the ØC was correlated to the Sirdal Magmatic Belt (SMB) located southeast of the ØC. Thus, the Precambrian evolution of the Øygarden Complex was differentiated from the Gothian (1,66-1,52 Ga) Western Gneiss Region (WGR), which it was previously believed to correlate (Bering, 1984).

Øygarden Complex consist of granitic, granodioritic and tonalitic gneisses and amphibolites, which have been affected by several phases of reworking (Sturt et al. 1975) Though, remnants of previous deformation events can still be found, the majority of visible strain in the Øygarden Complex today is a result of the most recent orogeny: the Caledonian (Sturt et al., 1975; Fossen and Dunlap 1998; Fossen and Rykkelid, 1990). Examples are stretching lineation and S/L-fabrics that are interpreted to have formed by the eastward Caledonian nappe translation and the subsequent westward backsliding of the orogenic wedge (Fossen and Rykkelid 1990; Larsen et al., 2003). Furthermore several N-S and E-W trending antiforms developed following the Caledonian orogeny, which affect the character of the gneiss fabric in the Øygarden Complex (Larsen et al., 2003). Sotra is positioned on the eastern limb of the N-S trending Sotra-Fedje culmination, resulting in a general trend of eastward dipping and plunging foliation and lineation, locally disturbed by E-W trending Sotra- and Sund Antiform (Larsen et al. 2003). After reaching the brittle-ductile transition zone at c. 396

Ma brittle faults and fractures developed throughout the Øygarden Complex as two main fracture sets trending NE-SW and NW-SE (Larsen et al., 2003).

The next sections further describe the characteristics of the Øygarden Complex's evolution divided into Pre-Caledonian-, Caledonian- and Post-Caledonian events.

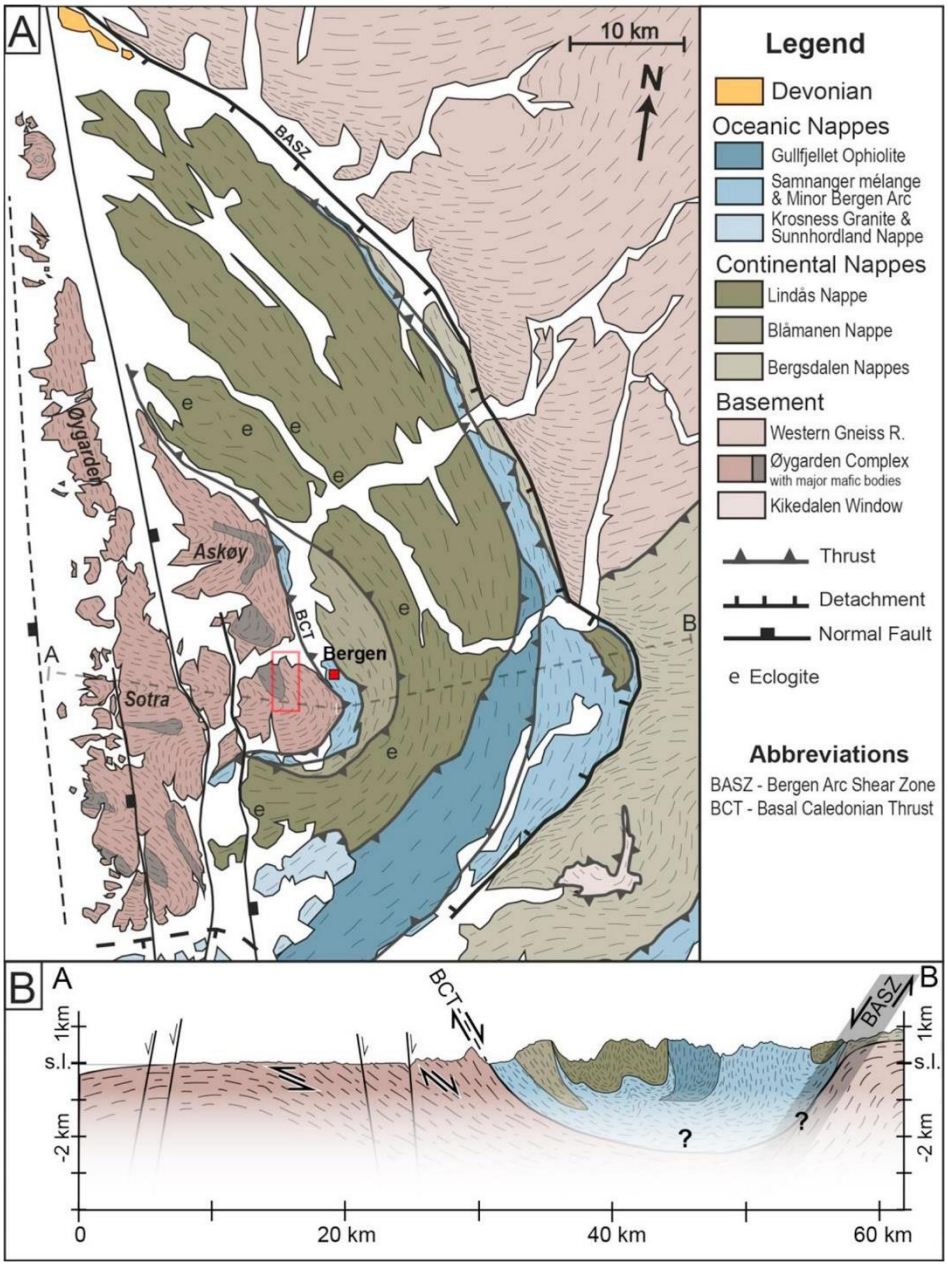


**Figure 3.1-1 A) Position of the Øygarden Complex in the centre of the Bergen Arc System B) Illustrates the large-scale N-S trending anticline and how the Caledonian thrust nappes occupy a depression in the basement complex related to the Basal Caledonian Thrust and Bergen Arc Shear zone. From Wiest et al. (2018).**

## 3.2 Pre-Caledonian

During Precambrian Baltica (Scandinavia) was a part of the Archean and Paleoproterozoic terrane Fennoscandia (Torsvik and Cocks, 2005) that docked with the two segments Sarmatia and Volgo-Uralia and formed the East European Craton (EEC), which constitutes the northeastern half of the present European continent (Boganova et al., 2008). Subsequently as the formation of EEC, amalgamation of the supercontinent Columbia took place, and the (present-day) southwest margin of Fennoscandia was probably located at the margin of the supercontinent (Roberts and Slagstad, 2015). Whether Columbia broke up completely before the amalgamation of the subsequent supercontinent Rodinia is a subject of debate (Roberts and Slagstad, 2015).

In models of the assembly of Rodinia, Fennoscandia is traditionally placed within the interior, and the Sveconorwegian orogeny regarded as an eastern continuation of the Grenville orogens in Canada (Roberts & Slagstad 2015, Slagstad et al. 2013). However, as reconstructing the assembly of Precambrian supercontinents is challenging due to e.g. overprinting by later geologic events and poor palaeomagnetic data (Slagstad et al., 2013) multiple configurations of Rodinia are proposed and possible as discussed by Corfu et al. (2014). The late-Mesoproterozoic Sveconorwegian orogen in (present-day) Scandinavia is divided into five lithotectonic units: the parautochthonous Eastern segment and the tectonically transported terranes: Idefjorden, Kongsberg, Bamble and Telemarkia (Bingen et al., 2008). U-Pb zircon geochronology published by Wiest et al. (2018) classifies the Øygarden Complex as part of the Telemarkia terrane, which formed during a short (1,52-1,48 Ga) voluminous magmatic event (Bingen et al., 2005). Whether Telemarkia is endemic or exotic to Fennoscandia is debated, however Telemarkia and the Bamble-Kongsberg terrane encompass Archean and Paleoproterozoic zircons in sedimentary deposits, which are indications of a position at the margin of an evolved craton in the Mesoproterozoic (Bingen et al., 2005, 2008).

Although there are discussions related to the style of the late Mesoproterozoic Sveconorwegian orogeny, the orogeny is traditionally regarded as a result of a collision including the continents Laurentia (Greenland), Baltica (Scandinavia) and (possibly) Amazonia (Bingen et al., 2008; Slagstad et al., 2017). Bingen et al. (2008) presented a model of the Sveconorwegian orogeny based on continent-continent collision, which was later challenged by Slagstad et al. (2017), who proposed a non-collisional accretionary orogeny. Findings in the study of eastern Øygarden Complex by Wiest et al. (2018) support an

accretionary model of the orogeny, however the findings do not eliminate the model by Cawood and Pisarevsky (2017) who suggested a clockwise rotation of Baltica and a soft collision with Amazonia.

Break-up of the supercontinent Rodinia initiated about 800 Ma, and it is from this dismantling, and separation from Laurentia by the opening of the Iapetus Ocean c. 500 Ma, that Baltica came to as an independent continent (Torsvik and Cocks, 2005).

## 3.3 Caledonian Orogeny

When the formation of the Iapetus Ocean initiated, present-day Norway was geographically inverted compared to the position today and located on the eastern margin of Baltica (Corfu et al., 2014). After reaching its widest extent in Early Ordovician (c. 480 Ma) (Torsvik and Cocks, 2005, and references therein), subduction at both margins gradually closed the Iapetus Ocean, which resulted in a Silurian to early Devonian collision between Baltica and Laurentia and the following Caledonian orogeny (Andersen et al. 1990 read in Andersen et al 91, Fossen and Rykkelid 1992b; Roberts, 2003, Torsvik and Cocks, 2005; Fossen and Dunlap 2006; Gee et al., 2008; Corfu et al., 2014). Baltica rotated counter-clockwise towards its present orientation, positioning Norway on the western margin facing the approaching Laurentian plate (Torsvik and Cocks, 2005). The gradual closing of the Iapetus Ocean and a rotating Baltica eventually led to an oblique continent-continent collision between Baltica and Laurentia c.430 Ma (Corfu et al., 2014 and references therein) in what is termed the Scandian phase of the Caledonian orogeny(Figure 3.3-1) (Roberts 2003, Gee 1975 read in Fossen & Dunlap 2006).

The Scandinavian Caledonides are characterized by a series of thrust nappes translated hundreds of kilometres onto Baltica as the Baltican margin was subducted below Laurentia (Andersen et al., 1991; Fossen and Dunlap, 1998; Roberts, 2003; Corfu et al., 2014). During the Caledonian thrusting, metasedimentary rocks from Precambrian to lower Paleozoic deposited onto the Baltic shield acted as a weak décollement zone enabling the immense nappe translation (Fossen, 1992; Fossen and Rykkelid 1992a, 1992b). As the basement in western Baltica, e.g. Øygarden Complex, was affected by Caledonian deformation, the western Caledonian orogen is classified as thick skinned, although the orogeny is generally classified as thin skinned (Fossen and Rykkelid 1992b; Fossen & Dunlap 1998).

Commonly the Caledonian nappes are divided into four allochthonous units based on the techtonostratigraphy following Gee et al. (1985). Upward increasing nappe displacement is generally acknowledged, with the lowermost allochthon interpreted to have a Baltic affinity, while the uppermost is derived from Laurentia (Gee et al., 2008). However, more recent studies, e.g. Corfu et al. (2014), argue that with a better understanding of the tectonic units this tectonostratigraphic framework have become too simplistic,, and they instead suggest to describe the Caledonian nappes by differentiating between three segments; southern, central and northern.

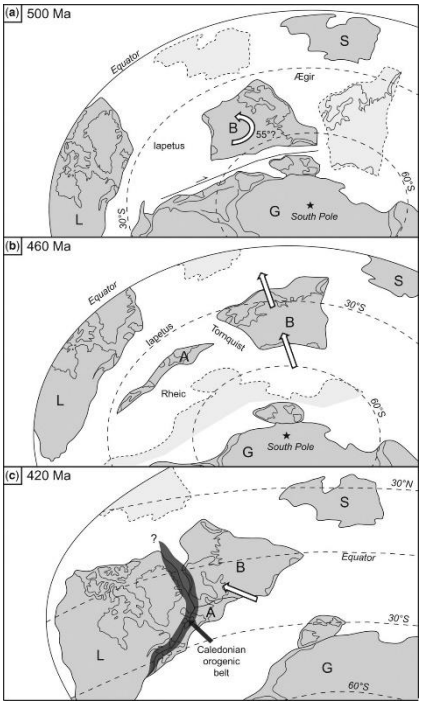


**Figure 3.3-1 Illustration of the closing of the Iapetus Ocean and continent continent collision between Baltica (B), Laurentia (L) and Amazonia (A) and timing of the events in the upper left corner a-b) Anti-clockwise rotation of Baltica. From Corfu et al. (2014)**

## 3.4 Post-orogenic Extension

Various models of the extension deformation have been suggested. Based on observations in the basal décollement in the Bergen area, Fossen and Rykkelid (1992b) interpreted the extension deformation as post-orogenic, and a result of divergent plate motions as opposed to the previously syn-collisional model proposed by Andersen and Jamtveit (1990) where extension deformation was explained by gravitational collapse of overthickened crust. Ar/Ar geochronology has indicated that the change from a contractional to extensional setting might have occurred around 410-400 Ma (Fossen and Dunlap, 1998).

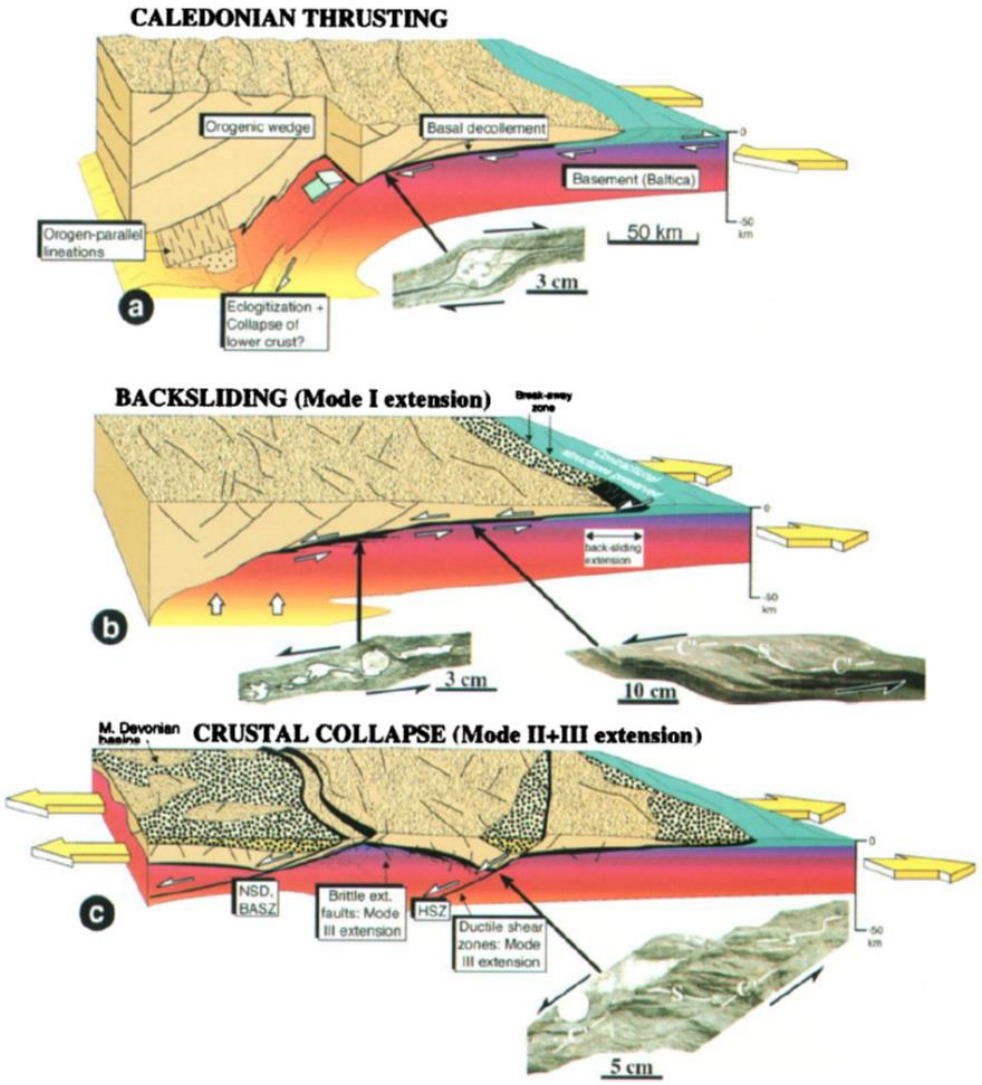


**Figure 3.4-1 Conceptual model for the structural and kinematic situation in western Norway from the Caledonian thrusting in a, to the backsliding of the orogenic wedge (b)and crustal collapse (c). Additional images show structures formed during each mode. From Fossen 2000**

Thermochronological data has shown that both Caledonian subduction and the subsequent exhumation to upper crustal levels were rapid processes, where the Øygarden Complex in a period of c. 10 myr cooled from amphibolite- through greenschist facies until reaching the brittle-ductile transition zone in Middle Devonian (c. 396 Ma) (Boundy et al., 1996; Larsen et al., 2003). Hence, the post-Caledonian deformation in the Øygarden Complex is characterised by a transition from ductile to semi-ductile and brittle deformation reflecting the gradual uplift from mid-crustal levels to the surface (Fossen, 1998).

On a regional scale the post-Caledonian deformation history is subdivided into four tectonic phases, where phase 3 and 4 are commonly ascribed to Mesozoic rifting and separation of Baltica and Laurentia by the formation of the North Atlantic Ocean. Furthermore, the Devonian post-orogenic extension in the Øygarden Complex can be explained three modes of deformation (Figure 3.4-2) (Fossen, 1992; Fossen, 2000; Fossen and Dunlap, 1998).

Reactivation of the basal décollement and backsliding of the allochthons to the northwest is the earliest indication of extensional deformation, hence, named Mode I (Figure 3.4-1) (Fossen, 1992). Stretching of the crust proceeded with the development of major hinterland dipping extensional shear zones, e.g. Nordfjord-Sogn detachment zone and the Bergen Arc Shear Zone (Mode II) (Fossen, 1992; Larsen et al., 2003). Similar extensional setting as in Mode II persisted throughout the Mode III phase. However, during this phase the crust reached the brittle-ductile transition zone in Mid Devonian time, which resulted in development of brittle faults with semiductile elements (Fossen, 2000; Larsen et al. 2003).

Larsen et al. (2003) identified two main sets of post-Caledonian faults and fractures in the Øygarden Complex (Figure 3.4-2 and Figure 3.4-3). These two sets formed after the hinterland directed shearing and a phase of large-scale folding during the Devonian. Set I and II are mainly differentiated based on their trend and mineralizations. Set I reflects a NW-SE extensional setting, and is characterised by hydrothermal alteration of the rock and epidote-, quartz- and chlorite mineralizations. Fractures in the younger set II are trending between N-S and NW-SE, indicating E-W extension, and characterised by calcite mineralizations. However, while epidote is confined to fractures of set I, calcite is found to occur in both sets. Relative age determinations determined that the calcite mineralization was younger than the epidote, indicating reactivation of set I during the formation of set II fractures.

As observed both north and south of Bergen, N-S trending Permian dikes are also present in the Øygarden Complex (Fossen, 1998; Larsen et al. 2003, and references therein). Hence, the E-W extension, which led to reactivation of, and dike intrusions in set II fractures, is interpreted as a regional shift in extension setting (Fossen, 1998; Larsen et al. 2003). Intrusions of Permian dikes and the following reactivation of pre-existing structures and formation of incohesive fault rocks from late-Jurassic time are commonly ascribed to Mesozoic rifting in the North Sea (Larsen et al., 2003, and references therein).

Exhumation history following the Devonian extension is debated, and contrasting models of erosion of the Caledonian orogeny and Censozoic uplift have been suggested (Nielsen et al., 2009; Ksienzyk, 2014).

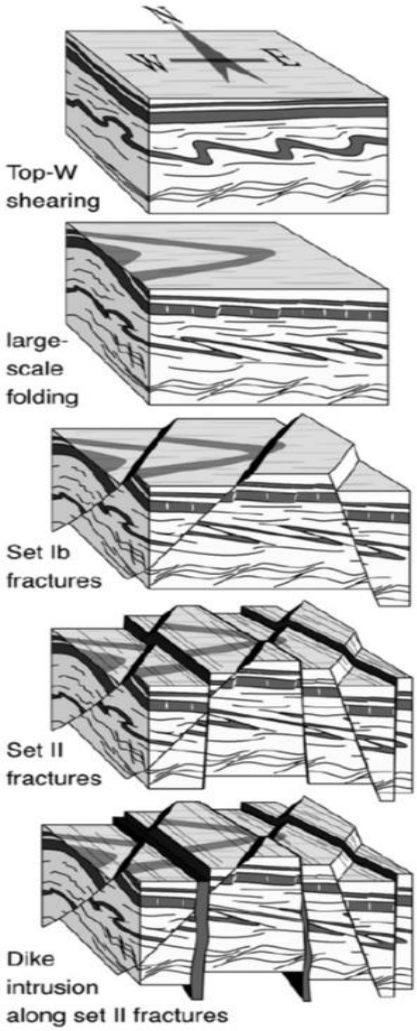


**Figure 3.4-2 The post-Caledonian tectonic development of the Øygarden Complex from Larsen et al. (2003).**

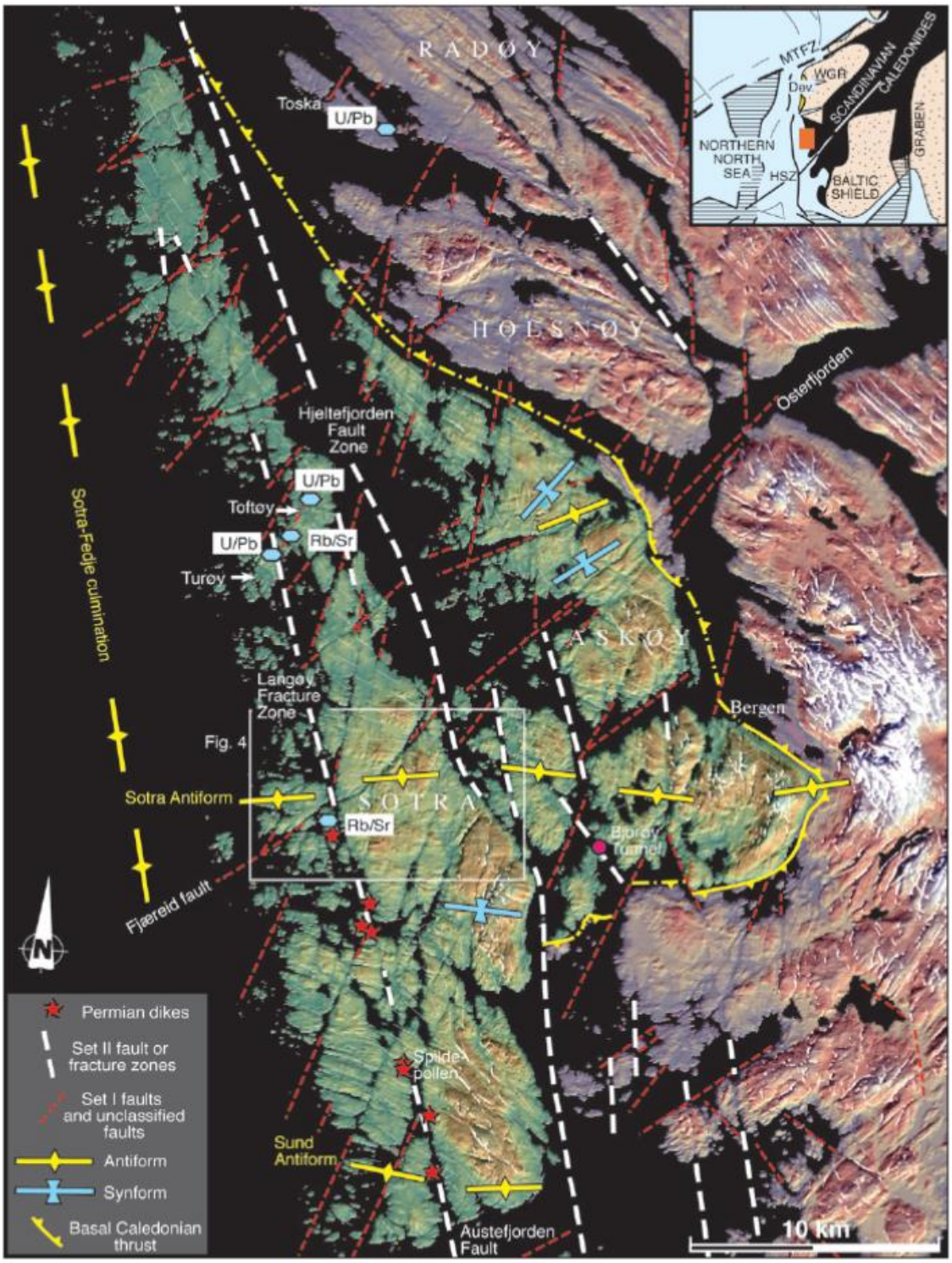


**Figure 3.4-3 Map of Sotra showing the N-S and E-W trending antiforms and set I and II fractures described in text. From Larsen et al. (2003)**

# 4 METHODS

The methodology of this study consists of the two main components fieldwork and lineament mapping of orthophotos and UAV images. By applying this methodology attributes from a large number of fracture lineaments assessed at different scales can be analysed to create a basis for describing and characterizing fracture corridors and spatial distribution of properties.

## 4.1 Fieldwork

As fracture corridors often generate topographic depressions, the accessibility to outcrops may be limited by steep valley sides and vegetation (Gabrielsen and Braathen, 2014). Thus, the exposed fracture corridors on the western coast of Sotra are excellent outcrops as they enable the distribution of attributes to be studied, both along and across the corridors. Fieldwork was conducted in the Precambrian basement complex, named the Øygarden Complex, on Sotra (Sturt et al., 1975). During four weeks of fieldwork fracture sampling was conducted at four sites: Golta, Nesvika, Straume and Viksøy (Figure 4.1-1), with the purpose of assessing fracture attributes, fracture frequency and connectivity.

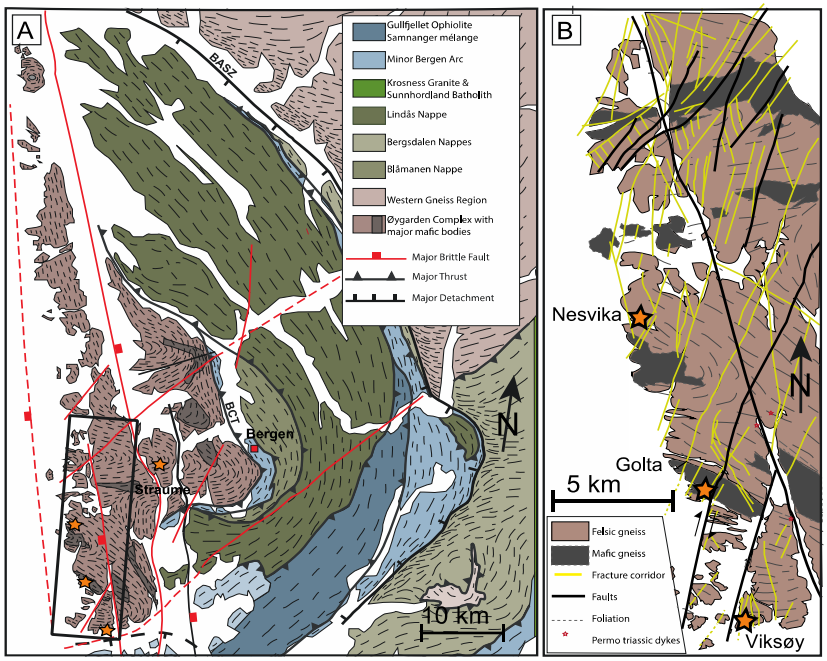


**Figure 4.1-1 Field locations marked on a geological map of the Bergen Arc System by Wiest et al. 2018. A) Show th position of the Øygarden Complex in the centre of the Bergen Arc System. Field location Straume just east of the box that marks the area of B) Field locations Nesvika, Golta and Viksøy.**

### 4.1.1 Linear scanline

The linear scanline method includes sampling the number of fractures that intersect a line (Figure 4.1-2, Figure 4.1-3), and has been widely used to estimate fracture intensity (Hudson Priest 1983). However, estimations of intensity and spacing based on linear scanlines are biased by the relative orientation of the fractures to the scanline, as fracture sets with low angles to the scanline would be undersampled compared to fractures with higher angles (Terzaghi, 1965). Hence, various authors have proposed different methods of fracture sampling to avoid this orientation bias. For example, Watkins et al. (2015) suggests using a circular scanline combined with areal sampling in areas of heterogeneous fractures instead of linear scanlines. For this study, the linear scanline method has been applied as it is an effective sampling method, and to characterize the distribution of fracturing across fracture corridors. To account for the orientation bias the obtained data has been corrected following Terzaghi (1965) (see section 4.1.2).

20 linear scanlines were sampled, 11 positioned in fracture corridors and 8 in the background area (outside of corridor). The scanlines were positioned horizontal and oriented approximately perpendicular to the trend of fracture sets and to the long axis of the fracture corridor (Figure 4.1-2).

In addition to histograms illustrating the spatial distribution of fractures, stick-plots and cumulative frequency diagrams were created following the methods proposed by Sanderson

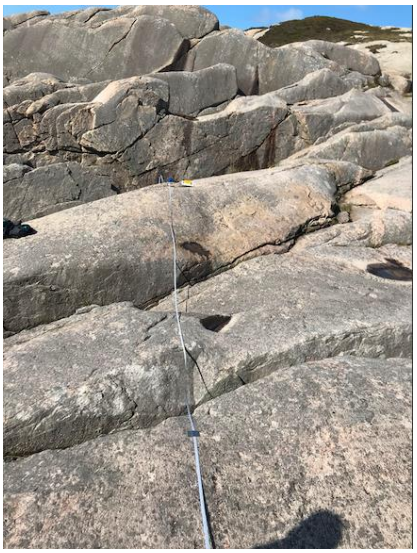

**Figure 4.1-2 Linear scanline from the field loclity Nesvika. The scanlineis oriented approximately perpendicular to the dominating fracture set. Photo: Eirin Hermansen**

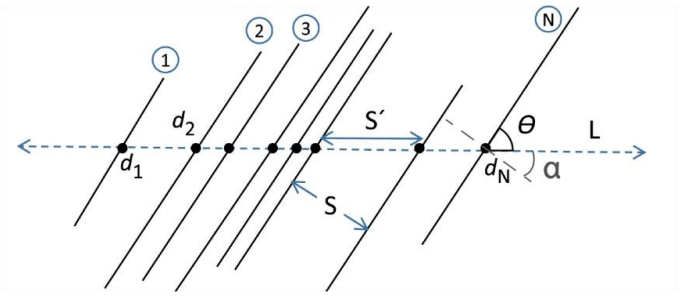


**Figure 4.1-3 Concept and terminology associated with linear scanlines. Intersections between fractures and scanline termed $d_1$, $d_2$, $d_3$, $d_i$....$d_N$. Θ is the angle between the scanline and the fracture, which in terms is used to find α (the angle between the scanline and the line perpendicular to the fracture). Slightly modified from Sanderson and Peacock (2019).**

and Peacock (2019). Presenting the fracture frequency by stick-plots is in some cases preferred over the use of histograms, as the stick-plot does not degrade the raw data by binning it, but preserve the intersection point of each fracture.

### 4.1.2 Fracture frequency and intensity

As each intersection between a fracture and the scanline was recorded, the fracture intensity, which in one dimension is equal to the fracture frequency (mean number of fractures per unit length). Fracture intensity is estimated based on the sum of fracture lengths within an area, and is further explained in chapter 4.2.1. As mentioned in section 4.1.1, the linear scanline method produces an orientation and spacing bias (Terzaghi, 1965). To measure the true spacing and frequency of a fracture set, the scanline should be oriented perpendicular to the fractures (Terzaghi, 1965). If non-parallel fracture sets intersect the same scanline, only the apparent spacing and frequency can be measured directly. To avoid undersampling of fractures not normal to the scanline, the data is corrected following Terzaghi (1965).

Fracture frequency (F) is estimated by the equation; $F = N/L*\cos\alpha$ ($P_{10}$ in Sanderson and Nixon, 2015). Where N is the number of fractures of a distinct set that intersect the scanline, L is the total length of the scanline and α the angle between the scanline and a line perpendicular to the fracture (Figure 4.1-3). The frequency is first estimated for each individual fracture set, and frequency along the scanline can then be found by adding these individual estimations (Hudson and Priest, 1983).

### 4.1.3 Potential sources of error

The methods of attribute sampling along linear scanlines induce some potential sources of error. Firstly, the orientation bias created by the relative angle between the scanline and the fracture, which may affect the estimations of fracture frequency. Furthermore, all fracture orientations were sampled using a geological compass, which may introduce errors related to inaccurate readings and estimations of the orientations of fractures that were not accessible. Areas covered in vegetation also limited the access for sampling attributes, which may affect the fracture frequency as no fractures were sampled, but may have been present beneath the vegetation. Due to the topography of the fracture corridors, sampling along the same scanline was at times conducted at different heights. This may have caused some inaccurate measurements of intersection points. Fracture trace length was sampled when possible. However, it is challenging to measure the trace length accurately as it is uncertain if the

observed length observed in the outcrop is the true length of the fracture (Singhal and Gupta, 2010).

## 4.2 Lineament mapping

To characterize the spatial distribution of fracture attributes, manual lineament mapping was conducted based on remote sensing imagery in the software ArcGIS. Regional lineaments were mapped using orthophotos of the field area obtained from *Norgeibilder.no.* Furthermore, detailed mapping and topology analyses of the field locations Nesvika and Tofterøy were enabled by high-resolution UAV (unmanned aerial vehicle) images collected using a DJI Phantom 4Pro drone.

Digitization of the fracture traces was conducted in ArcGIS by creating a new polyline shapefile, and using the *editor* and *snapping tool* to draw fractures as lines following the interpreted fractures on the images. Utilizing the snapping tool ensured that all intersections between fractures were registered, which is fundamental to characterise the connectivity of the network (Nyberg et al 2018). The benefit of digitizing the fracture network in ArcGIS is that, in addition to creating a georeferenced lineament map, information as orientation, trace length and connectivity of the fracture network can be extracted. Analyses of geometric and topological properties of the fracture network were conducted using Network GT (Network Geometry and Topology), a toolbox for ArcGIS (Nyberg, et al 2018).

### 4.2.1 Network GT

Network GT (Network Geometry and Topology) is an open-source ArcGIS toolbox developed to incorporate topological properties in the analyses of two-dimensional fracture networks (Nyberg et al 2018). Topology, as explained in section 2.4 , is essential when estimating the connectivity and characterizing the fluid flow properties of a fracture network (Sanderson and Nixon, 2015; Nyberg et al., 2018). The fractures are represented by the components: lines, branches and nodes (Figure 4.2-2). By registering connections per branch ($C_B$) a quantitative measure of connectivity can be estimated by a number from 0 to 2 (as branches are bounded by two nodes, $C_B$ can not be greater than 2) (Nyberg et al., 2018). $C_B$ is calculated by the equation:

$$C_B = (3N_Y+4N_X)/N_B$$

Where $N_Y$ is the number of Y-nodes, $N_X$ is the number of X-nodes and $N_B$ is the total number of branches (Sanderson and Nixon, 2015). The resulting $C_B$ is a dimensionless number that indicates the connectivity of the network. Furthermore, the proportion of each type of nodes and branches is commonly presented in a ternary diagram, where $C_B$ is represented by a line, which makes it easy to derive the estimated connectivity of the network (Sanderson and Nixon, 2015).

An option in Network GT is to conduct a grid analysis of the digitized fracture network. This function enables the spatial variation of various geometric and topological properties to be assessed. Grid analyses were during this project utilized to create density maps showing how the 2D intensity ($\Sigma L/A$) (Figure 4.2-1 and $C_B$ varied through the networks. When creating the grid, a user defined size of the grid cell and additional search radius has to be determined. For the two digitized fracture networks a grid cell size of 3x3m and a search radius of 10m were selected. A more detailed description of the workflow in ArcGIS is provided in Appendix I.

### 4.2.2 Potential sources of error

Manual digital mapping of fractures is highly dependent on the resolution of the image, and the experience of the interpreter. Even with high-resolution UAV images of the outcrops, fewer fractures will likely be mapped than observed in outcrops by field investigations. Thus, the characterization of the fracture networks topology will depend on resolution even though the assessed topological parameters are dimensionless (Sanderson and Nixon, 2015). Due to the resolution limitation of this method, a fracture networks potential for conducting fluids will most likely be underestimated.

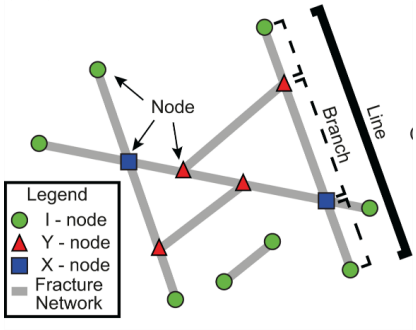


**Figure 4.2-2 Terminology associated with topology of fracture networks. From Nyberg et al. (2018)**

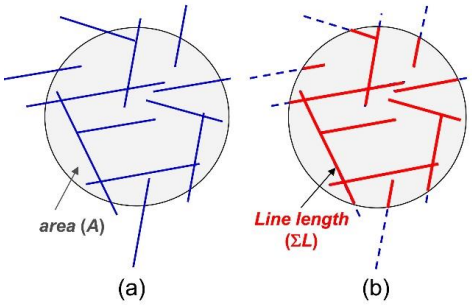


**Figure 4.2-1 Illustration of the concept behind the estimation of 2D intensity based on sum of line lengths within a sample area. From Sanderson and Nixon (2015)**

# 5 RESULTS

In this chapter the field based observations, digitized fracture network and the following analyses conducted to characterise the spatial arrangement (fracture geometry and topology, sensu Laubach et al., 2018) of fracture corridors is presented. The first section describes and characterise the large-scale structures in the field localities, while the latter part of the chapter describes the mapped fracture geometry and topology.

## 5.1 Study areas

Fracture sampling was conducted at four sites: Golta, Nesvika, Viksøy and Straume, which were selected based on accessibility to fracture corridor outcrops and lithology (quartz-feltspathic gneiss and amphibolite with variable gneiss-foliation). Furthermore, the possibility of sampling complete sections through corridors and the background area was emphasized during the selection of field localities. A total of six fracture corridors were analysed by field observations and high-resolution photogrammetry. Based on orthophotos, the widths of these corridors ranged from c. 10 to 40m, and lengths were in the scale of hundred meters to several kilometres.

Approximately 1500 fractures along 19 linear scanlines (described in section 4.1.1) were sampled. However, based on accessibility to the fractures, orientation was measured for c. 1300, and trace length for c. 900 of these 1500 fractures. All scanlines were oriented approximately perpendicular to the dominating fracture set and to the long axis of the fracture corridor. Thus, the scanlines were oriented E-W to NW-SE, as most fracture corridors trend NNE-SSW. Sample area and position of each scanline is indicated in Table 5.1-1 and the maps Figure 5.1-6 to Figure 5.1-10.

### 5.1.1 Fracture characterisation

In Nesvika, the bedrock consists of thick layers of massive, homogeneous quartz-feltspathic gneiss and zones of alternating amphibolitic and quartz-feltspathic layers. Foliation trends approximately E-W. Pegmatitic greisen structures, similar to the examples described on Bømlo by Schreiber and Viola (2017), is also common throughout the study area with an E-W orientation. Foliation and greisen structures could be traced across fractures and fracture

corridors with no visible displacement (Figure 5.1-4 E). Displacement was, however, in parts of the outcrops difficult to inspect, especially in Nesvika, partly due to lack of foliation banding in the gneiss. The majority of recorded fractures are therefore characterised as joints, with displacement only perpendicular to the fracture walls. Furthermore, Nesvika was characterised by en echelon patterns at an angle to the main strike of the corridors (Figure 5.1-5). These fractures occurred on a range of scales and created right stepping arrangements of overlapping, mostly isolated fractures. Contrary to the observations in Nesvika, fractures on Golta, Viksøy and Straume are characterised by mixed mode fractures and comprised displacement indications as slickenlines (Figure 5.1-3). A zone of red/pink coloured alteration of the host rock commonly occurred, often associated with fractures filled with green epidote (Figure 5.1-1). These features are common in the Øygarden Complex, and have been described by Fossen (1998) and Larsen et al. (2003) as a result of hydrothermal fluid circulation. Only 2,5% of the total database of fractures contained secondary mineralization or clay. Fractures with mineral fillings or clay were exclusively sampled from fracture corridors on Golta and Straume. Most common was green coloured epidote in NE-SW fractures (Figure 5.1-3). Less frequently quartz, calcite and chlorite was recorded, also within NE-SW trending fractures. Although, none of the fractures sampled along the scanline on Viksøy contained mineral fill, alteration was common. In Nesvika alteration and fracture infillings were absent in the sampled database.

**Figure 5.1-1 Red/pink alteration around en echelon arranged fractures in one of the field locations in Golta. Photo: Eirin Hermansen**

However, a few veins encompassed by alteration at one location close to one of the analysed corridors were observed (Figure 5.1-3 A and B).

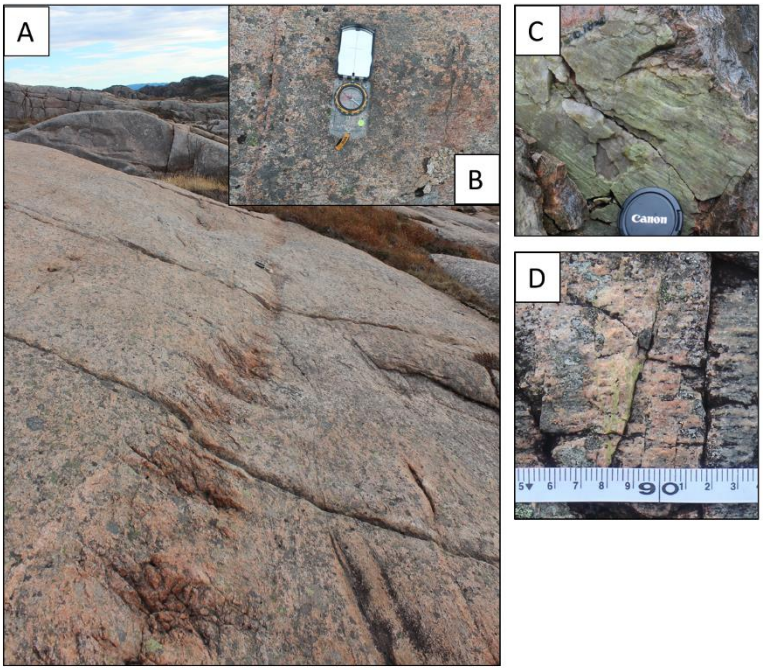


**Figure 5.1-3 A) Veins in background in field location Nesvika, view towards east. B) is a close up of the veins in A, with a quartz vein to the left and epidote vein to the right of the compass. Compass for scale in both images. C) slickenlines and green epidote from field locality Straume D) Green epidote in fractures in the Golta field locality. Photo: Eirin Hermansen**

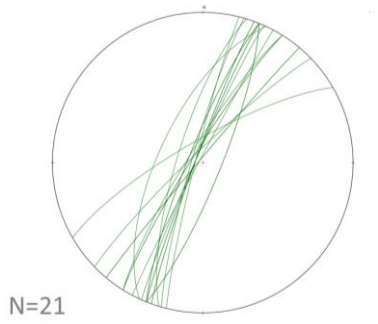


**Figure 5.1-2 Orientation of the 21 sampled fractures with green epidote. Made with OpenStereo software.**

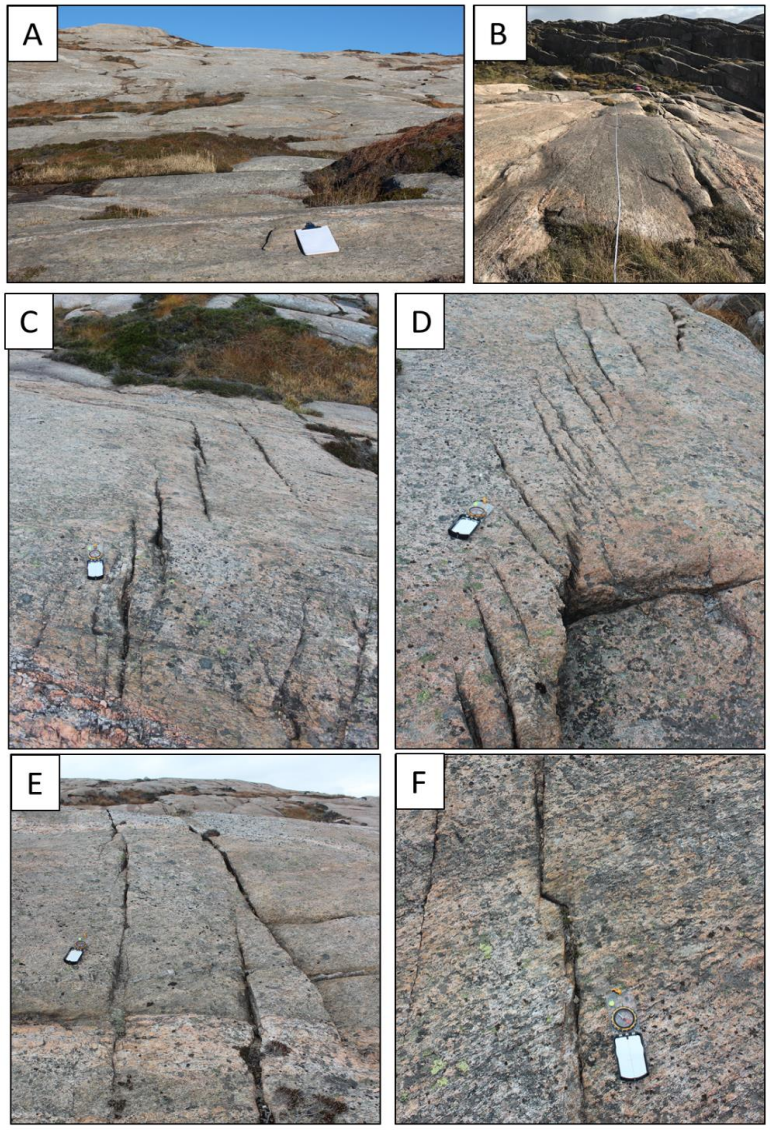


**Figure 5.1-4 Field photographs from the background in Nesvika. Photo: Eirin Hermansen**

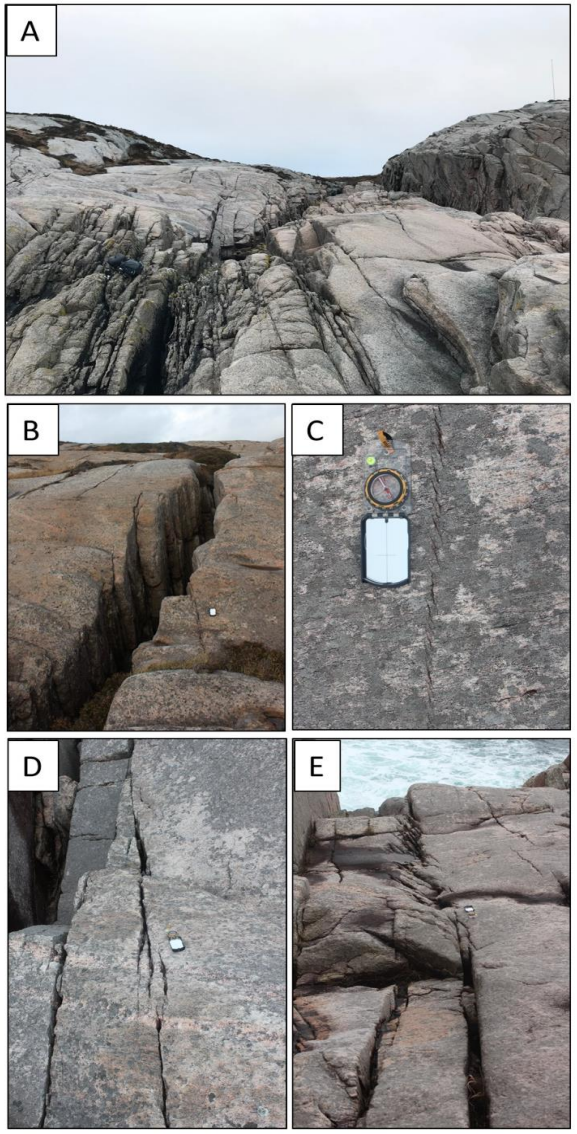


**Figure 5.1-5 Field photographs showing fracturing in fracture corridors A) Viksøy B-E) Nesvika. Photo: Eirin Hermansen**

**Table 5.1-1 Scanline ID and sample area**

| Scanline ID | Sample area |
|---|---|
| Golta A | Corridor |
| Golta B | Corridor |
| Golta C | Background |
| Golta D | Corridor |
| Golta E | Corridor |
| Golta F | Corridor |
| Nesvika A | Background |
| Nesvika B | Corridor |
| Nesvika C | Background |
| Nesvika D | Background |
| Nesvika E | Background |
| Nesvika F | Background |
| Nesvika G | Corridor |
| Nesvika H | Corridor |
| Nesvika I | Corridor |
| Nesvika J | Corridor |
| Nesvika K | Background |
| Straume | Corridor |
| Viksøy | Background |

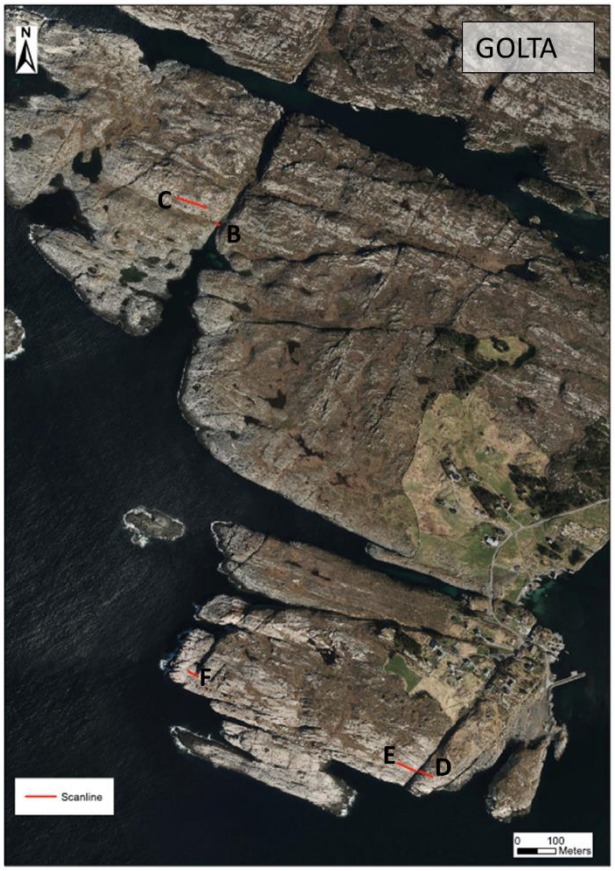


**Figure 5.1-7 Position of scanlines Golta B, C, D, E and F. Orthohoto from Norgeibilder.no**


**Figure 5.1-6 Position of scanline Golta A. Orthophoto from Norgeibilder.no**

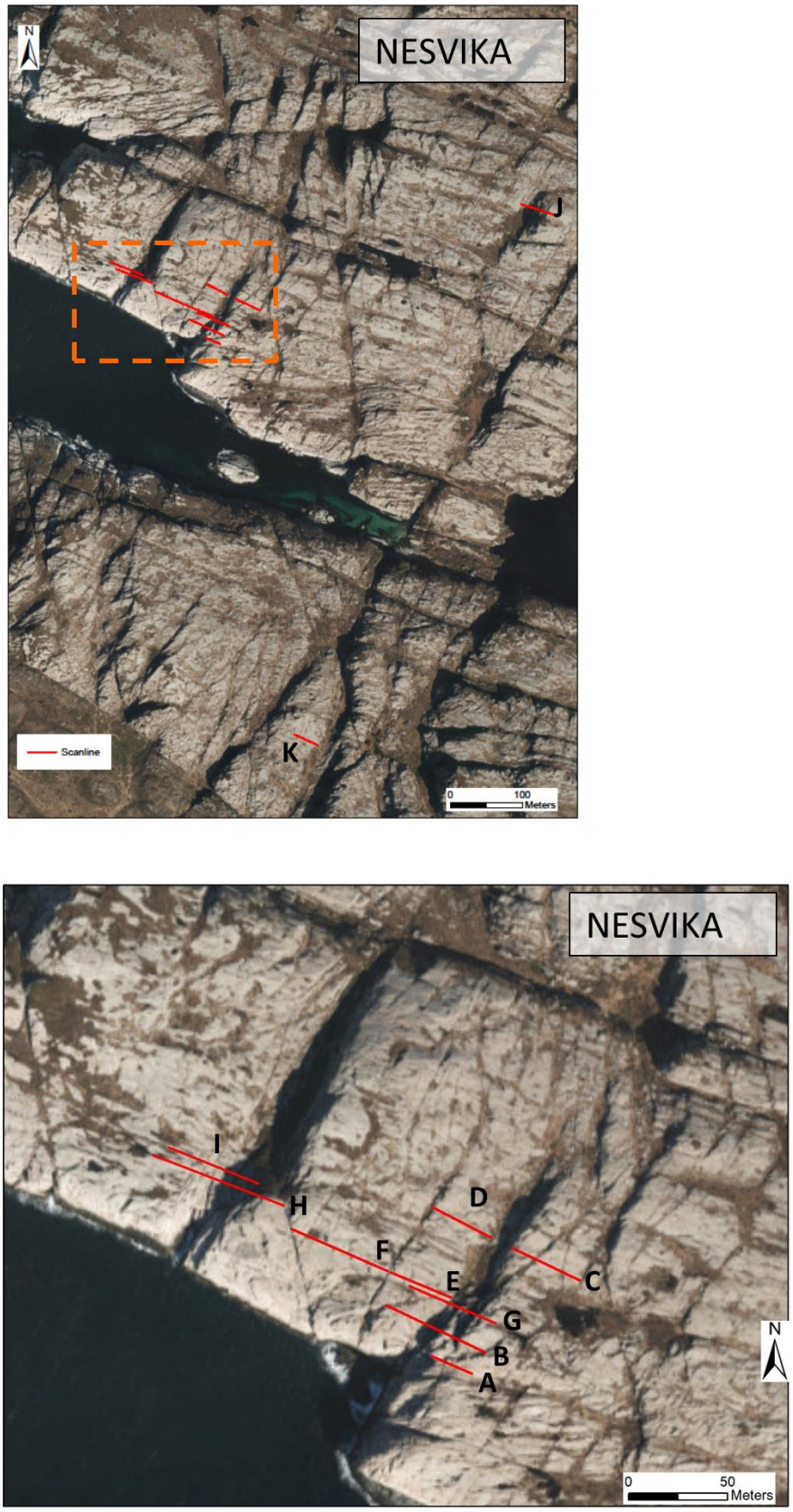


**Figure 5.1-8 Scanline positions in Nesvika. The area in orange stapled lines in the upper photo is enlargened in the lowermost image. Orthophotos from Norgeibilder.no**

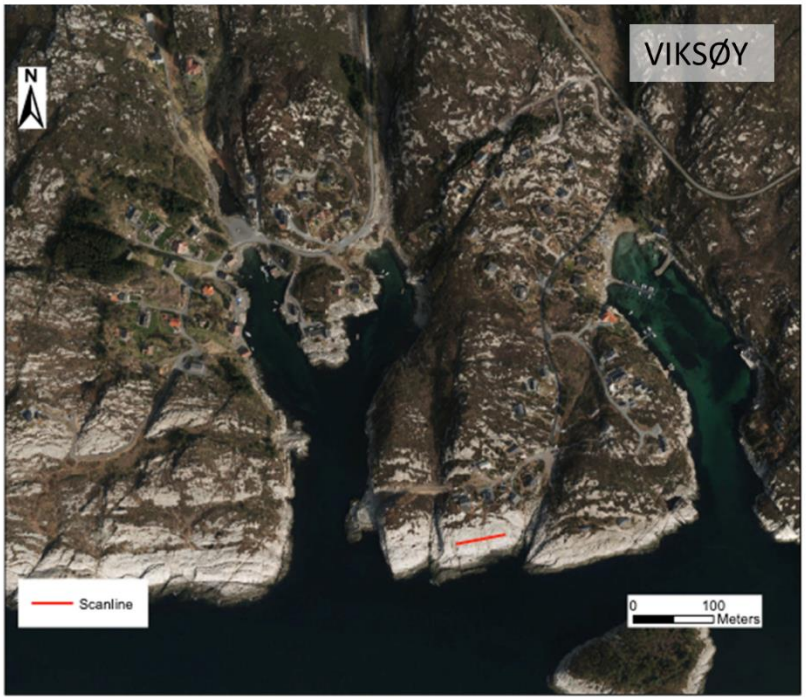


**Figure 5.1-9 Position of scanline on Viksøy. Orthophoto from Norgeibilder.no**

**Figure 5.1-10 Fracture corridor on field location Straume. Photo: Eirin Hermansen**

## 5.2 Spatial arrangement

### 5.2.1 Fracture Orientation

The investigated fracture corridors mainly consisted of steep, sub-parallel fractures (Figure 5.2-1). As can be seen on Figure 5.2-2 the dominating fracture set on the Golta, Nesvika and Straume locations had a NNE-SSW trend, thus, the majority of fractures comprising the fracture corridors were parallel to sub-parallel to the main lineament.

On Golta about 90% of the sampled fractures within fracture corridors had a NNE-SSW trend, while the background area recorded a significantly different distribution, comprising a wider range of orientations from NW-SE to NE-SW. Similar to the observations from Golta, the majority of fractures in the Nesvika location (c. 90% within both corridors and background) have a NNE-SSW to NE-SW trend; hence, parallel to the main strike of the fracture corridors. However, in Nesvika as well, a wider distribution of orientations is observed within the background area, contrary to the more homogeneous distribution within the corridors. The fracture corridor sampled on Straume showed a large variety of fracture orientations, although the dominating fracture set trends NNE-SSW, similar to the fracture corridors on Golta and in Nesvika. On the Viksøy location the dominating fracture set has a NW-SE trend (about 60% of the fractures are within 40 degrees of the dominating orientation).

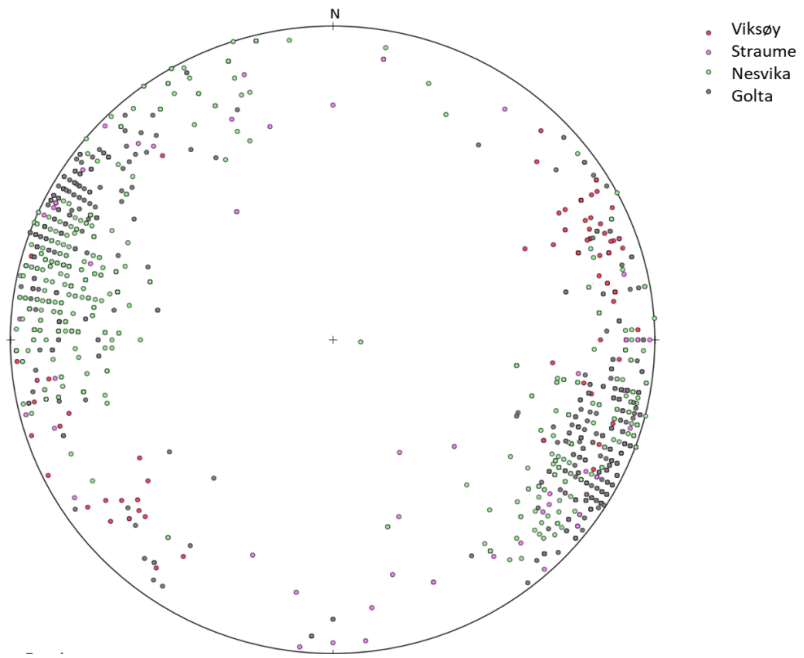


**Figure 5.2-1 Poles to fractures sampled at all field locations. Plot made in OpenStereo software.**

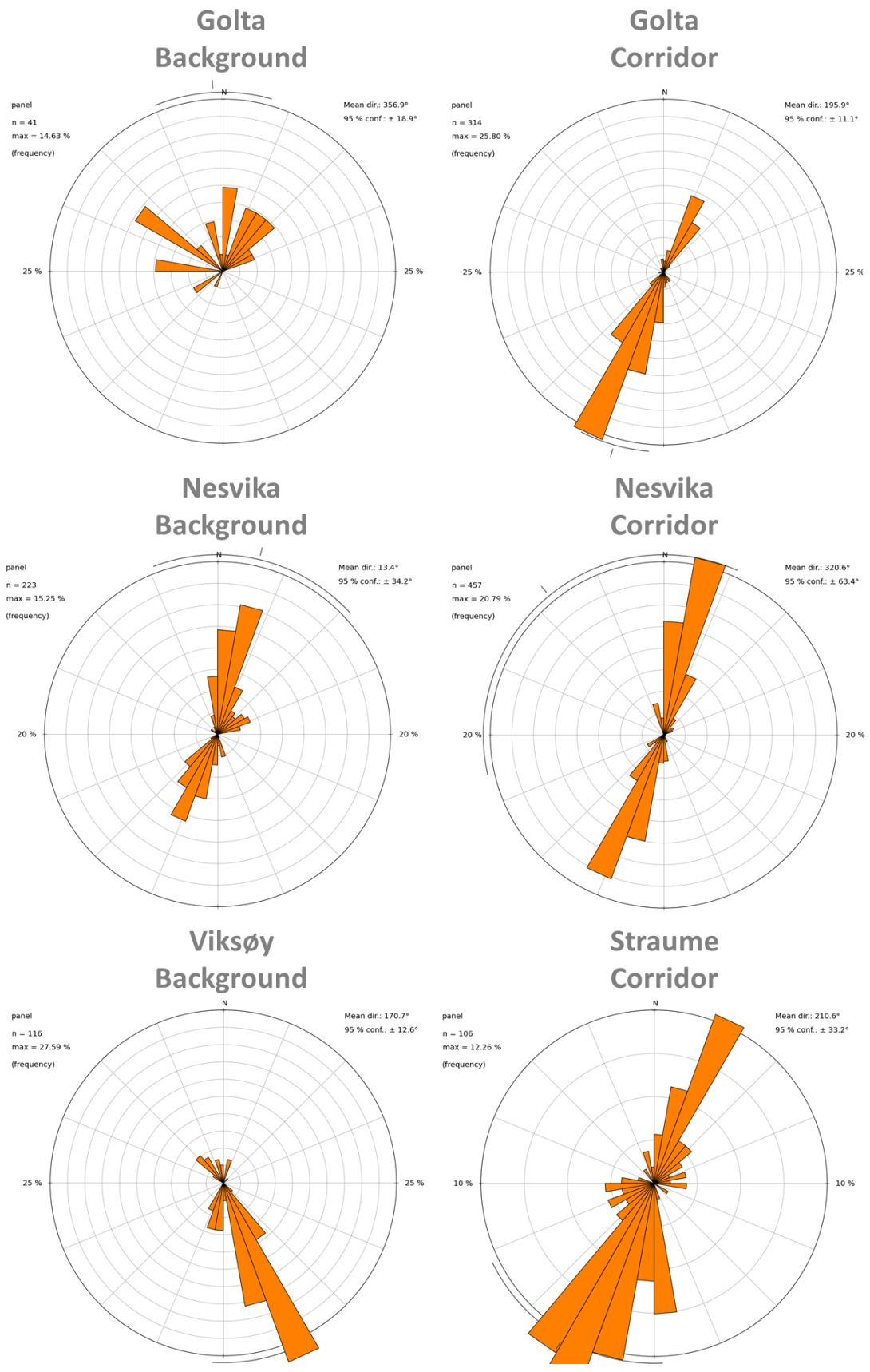


**Figure 5.2-2 Rose diagrams showing the orientations of fractures. Divided by field location and sample area. Made with the OpenStereo software.**

Fracture orientation was also extracted from the digitized fracture networks in the Nesvika and Viksøy locations. This method covered a larger area than what could be assessed by the linear scanlines, thus, there is a larger ratio of fractures from background to fracture corridor since the field mapping concentrated the measurements within or close to fracture corridors. Based on the digitized fractures from Nesvika, the NE-SW fracture set is dominating, although the NW-SE fracture set is more significant than what was observed from the scanline samples. Fracture orientations extracted from the digitized fracture network on Viksøy show the majority of fractures are trending between NNW-SSE to NW-SE, and that a minor NE-SW fracture set occur.

### 5.2.2 Trace length

The visible fracture trace length was measured along all scanlines, except Golta A and Straume that were sampled from vertical outcrops. As seen in Figure 5.2-3 the majority of fractures had trace lengths within 1 to 2 m, both within corridors and background. Longer trace lengths were recorded, but much less frequently, and none of the sampled fractures were longer than 30m. This indicates that both the corridors and the background area mostly contain short fractures. However, the trace length visible in outcrops is not necessarily the true length of the fracture, and a high degree of fracture segmentation was observed during

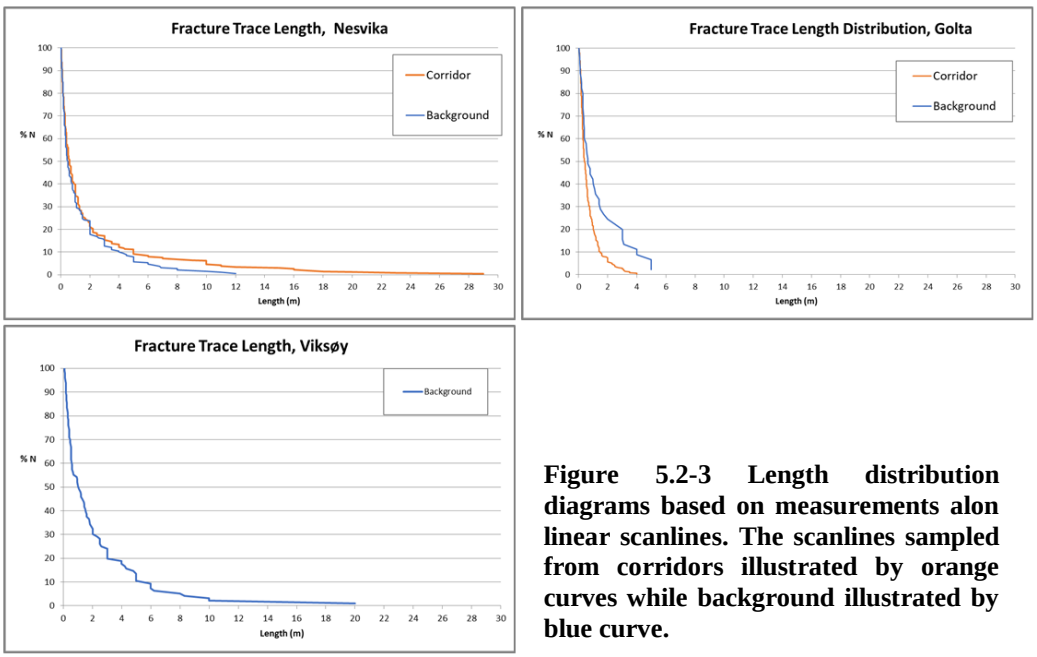


**Figure 5.2-3 Length distribution diagrams based on measurements alon linear scanlines. The scanlines sampled from corridors illustrated by orange curves while background illustrated by blue curve.**

field investigations, thus the effective length of the fracture may be longer than estimated herein.

### 5.2.3 Fracture frequency

Fracture frequency is estimated based on the number of fractures that intersect a set of linear scanlines (see section 4.1.1). Fracture frequency and fracture intensity are both commonly referred to as fracture density in literature. Herein, the term fracture frequency is used for the estimation of fracture abundance along the linear scanlines (one dimensional, number of fractures per length), while fracture intensity is used for estimations in 2D (sum of line length within an area). 11 scanlines were sampled within fracture corridors (inner scanlines), while 8 additional scanlines were sampled from the background (outside corridors) to establish a reference to the enhanced fracture frequency of corridors. The resulting fracture frequency of each scanline is presented in Table 5.2-1, ordered from sample area and increasing frequency. Furthermore, a set of histograms illustrates the distribution of fractures and fracture frequency along each scanline (Figure 5.2-4 and Figure 5.2-5).

**Table 5.2-1 Scanlines ordered by sample area and increasing fracture frequency showing the scanline length and sampled number of fractures.**

| Scanline ID | Length (m) | Fracture Nr. | Fracture Frequency F (fracture/m) |
|---|---|---|---|
| **Background** | | | |
| Nesvika D | 32.50 | 13 | 0.33 |
| Nesvika F | 47.32 | 22 | 0.44 |
| Golta C | 50.00 | 47 | 0.64 |
| Nesvika E | 34.52 | 27 | 0.74 |
| Nesvika A | 30.00 | 34 | 1.03 |
| Nesvika C | 38.55 | 42 | 1.05 |
| Nesvika K | 50.00 | 86 | 1.60 |
| Viksøy | 50.00 | 116 | 2.26 |
| **Corridor** | | | |
| Nesvika J | 50.00 | 49 | 0.97 |
| Nesvika G | 38.86 | 68 | 1.56 |
| Nesvika H | 39.24 | 87 | 2.16 |
| Golta E | 23.60 | 55 | 2.18 |
| Nesvika I | 26.05 | 67 | 2.50 |
| Golta B | 10.80 | 42 | 3.82 |
| Golta A | 48.50 | 235 | 4.16 |
| Golta F | 23.50 | 107 | 4.39 |
| Nesvika B | 39.70 | 189 | 4.56 |
| Golta D | 26.55 | 146 | 5.23 |
| Straume | 15.00 | 107 | 5.83 |

The background show fracture frequencies between 0,33 f/m and 2,26 f/m, while the frequencies from corridors range from 0,97 f/m to 5,83 f/m. On average the fracture frequency within the corridors on Sotra are four times higher than the background. A characteristic fracture frequency of fracture corridors could not be identified as four of the inner scanlines recorded lower frequency than the highest background value. Furthermore, the fracture frequency of both corridor and background seem to depend on field locality.

The Straume location recorded the highest corridor fracture frequency of 5,83 f/m, while the lowest frequencies (both background and corridor) were sampled in Nesvika. The corridors sampled in Nesvika show an average fracture frequencies three times greater than the background. A spatial variability of the fracture frequency was found both across- and along the strike of the corridor, as illustrated by the scanlines Nesvika B and G and as seen in Figure 5.2-7. Although these scanlines were parallel and only a few meters apart Nesvika B and G show estimated fracture frequencies of 4,56 f/m and 1,56 f/m, respectively. This may indicate a rapid change in fracturing within the corridors and/or short trace lengths.

Fracture corridors in Golta had frequencies ranging from 2,18 f/m to 5,23 f/m, which on average was about six times higher than the background area (0,64 f/m). Interestingly, a significant difference in fracture frequency was detected within the same corridor, where Golta D and E that were sampled. Golta D recorded an estimated frequency of 5,23 f/m while Golta E showed a frequency of 2,18 f/m. It was not possible to sample a continuous scanline across this particular corridor, as the innermost part was covered by water. Thus, the D and E scanlines were positioned vis-à-vis on opposite sides of the creek.

The highest background fracture frequency (2,26 f/m) was sampled at the southernmost field location, Viksøy, and is about two times the average background frequency. The Viksøy scanline was positioned between two fracture corridors, which have been previously assessed by Bastesen (in prep).

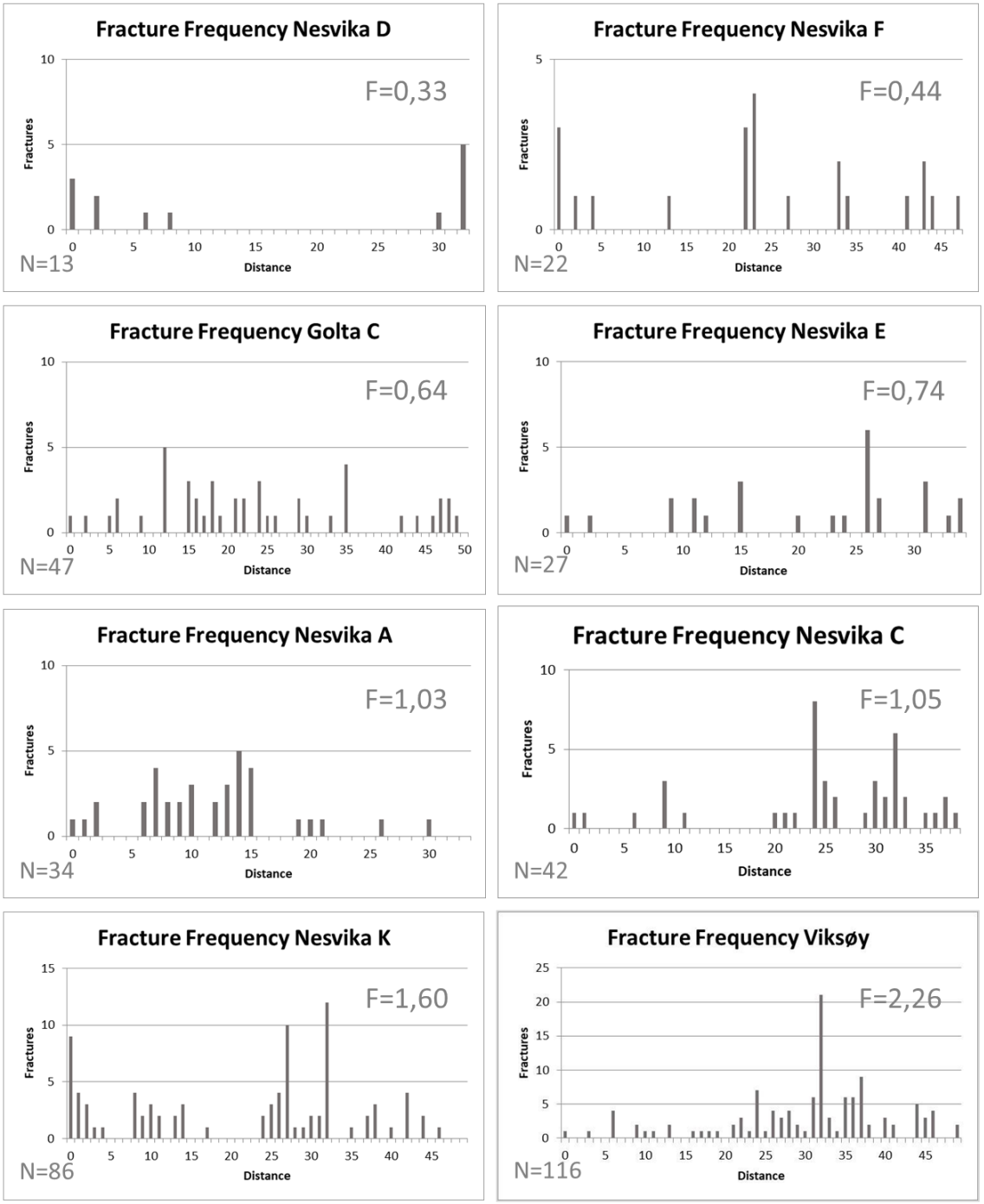


**Figure 5.2-4 Fracture frequency of background. Arranged by downwards increasing fracture frequency. Distance in meters. N indicates the number of sampled fractures along the scanline, and F the estimated fracture frequency.**

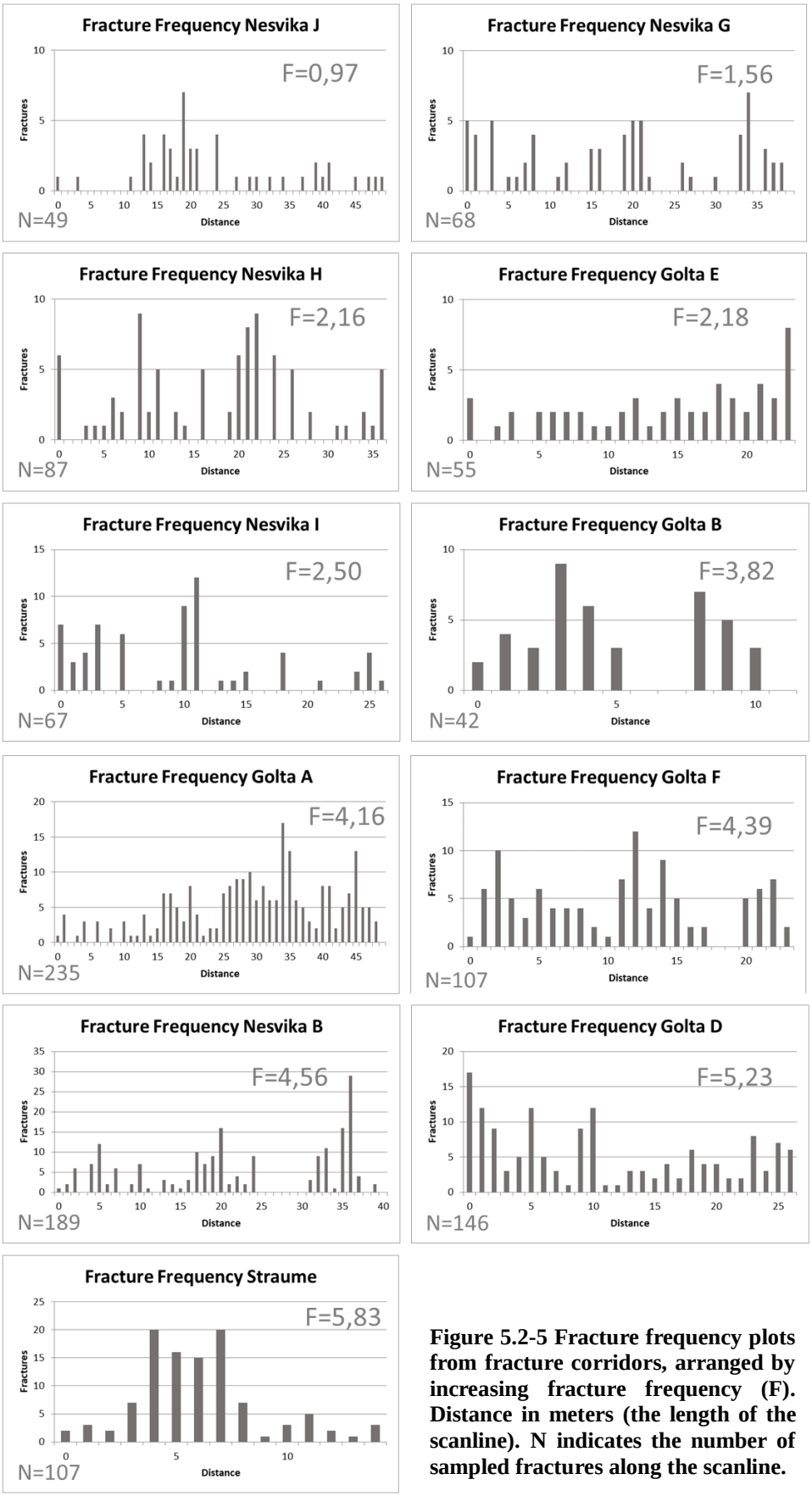


**Figure 5.2-5 Fracture frequency plots from fracture corridors, arranged by increasing fracture frequency (F). Distance in meters (the length of the scanline). N indicates the number of sampled fractures along the scanline.**

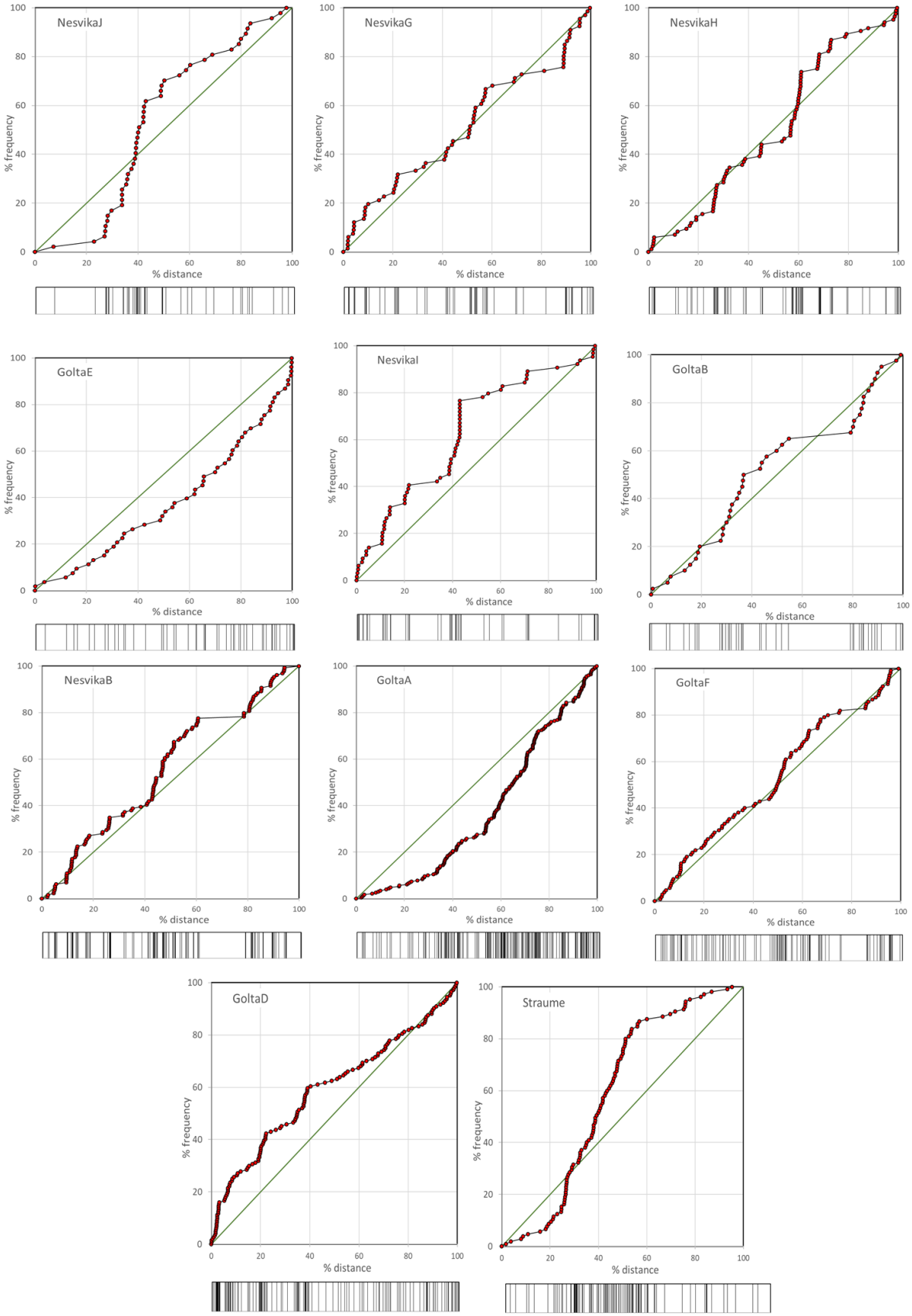


**Figure 5.2-6 Cumulative frequency and stick plots based on linear scanlines in fracture corridors. Arranged by downwards increasing fracture frequency as seen in table Table 5.2-1 and Figure 5.2-5. These plots were made using a spreadsheet developed by Prof. David J. Sanderson and David Peacock.**

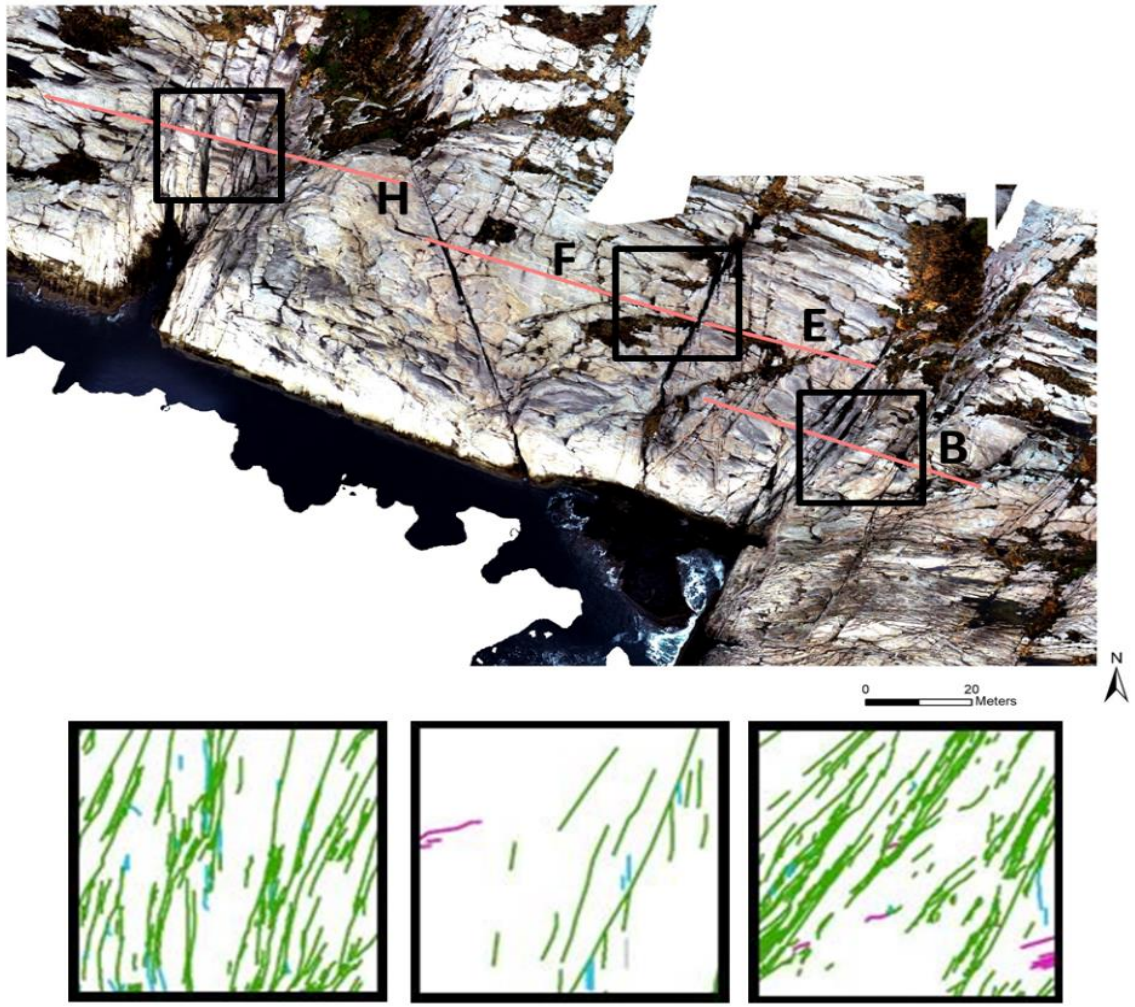


**Figure 5.2-7 UAV image of the field location Nesvika. The fracture intensity varies greatly over a distance of approximately 150 m as illustrated by the digitized fracture traces in the three boxes. Notice the en echelon pattern in the centered box, which is the same minor corridor as on Figure 5.1-5 B. Pink lines represent the position of the scanlines Nesvika B, E, F and H.**

### 5.2.4 Spatial distribution of fractures

Based on the frequency histograms (Figure 5.2-4 and Figure 5.2-5), density maps (fig Figure 5.2-9 and Figure 5.2-11), cumulative frequency diagrams and stick plots (Figure 5.2-6) the spatial distribution of fractures in fracture corridors was analysed.

Although histograms bin the data into intervals, they visually illustrate and quantify areas of higher fracture frequency. Based on these diagrams one can easily see that fractures were not evenly distributed along the scanlines. Furthermore, areas of higher fracture frequency stand out as peaks, and the frequency in distinct areas can be read of the diagram. Histograms based on the linear scanlines are in Figure 5.2-4 and Figure 5.2-5 ordered by sample area and increasing fracture frequency.

Because of the binning into intervals some authors prefer the use of stick plots as they do not degrade the raw data (Sanderson and Peacock, 2019). Stick plots are presented in Figure 5.2-6 with the cumulative frequency diagrams, which are plotted against normalized percentages of distance along the scanline from the first to the last sampled fracture. Fracture frequency is proportional to the slope of the curve. Thus, zones of higher frequencies are recognized by steeper slopes, which enable fracture clusters (zones where fractures are closely spaced) to be detected and quantified (Sanderson and Peacock, 2019). The majority of cumulative frequency diagrams based on inner scanlines (from fracture corridors) showed stair-stepped curves at various scales, indicating several clustered zones of varying fracture frequencies. Thus, the fractures are not evenly distributed throughout the corridors. Fracture corridors with This pattern was especially visible in the scanlines from the Nesvika location, which generally recorded lower fracture frequencies than the Golta, Straume and Viksøy locations. With increasing fracture frequency the fractures appear to be more uniformly distributed, showing a less distinct stair-stepped curve.

The density maps in fig (Figure 5.2-9 and Figure 5.2-11) show the spatial variability of 2D intensity ($\Sigma L/A$), based on the digitized fracture networks from the field localities Nesvika and Viksøy. These maps emphasize the difference between fracture corridors and background, as they cover a larger area than what could be assessed by the linear scanlines. From the density map a more significant variation in 2D intensity across the strike of the corridors than along strike can be inferred both in Nesvika and on Viksøy. The spatial distribution on Viksøy

show similar trends, but the across strike variation is less prominent than what was found in Nesvika. The along strike variation is also less distinct.

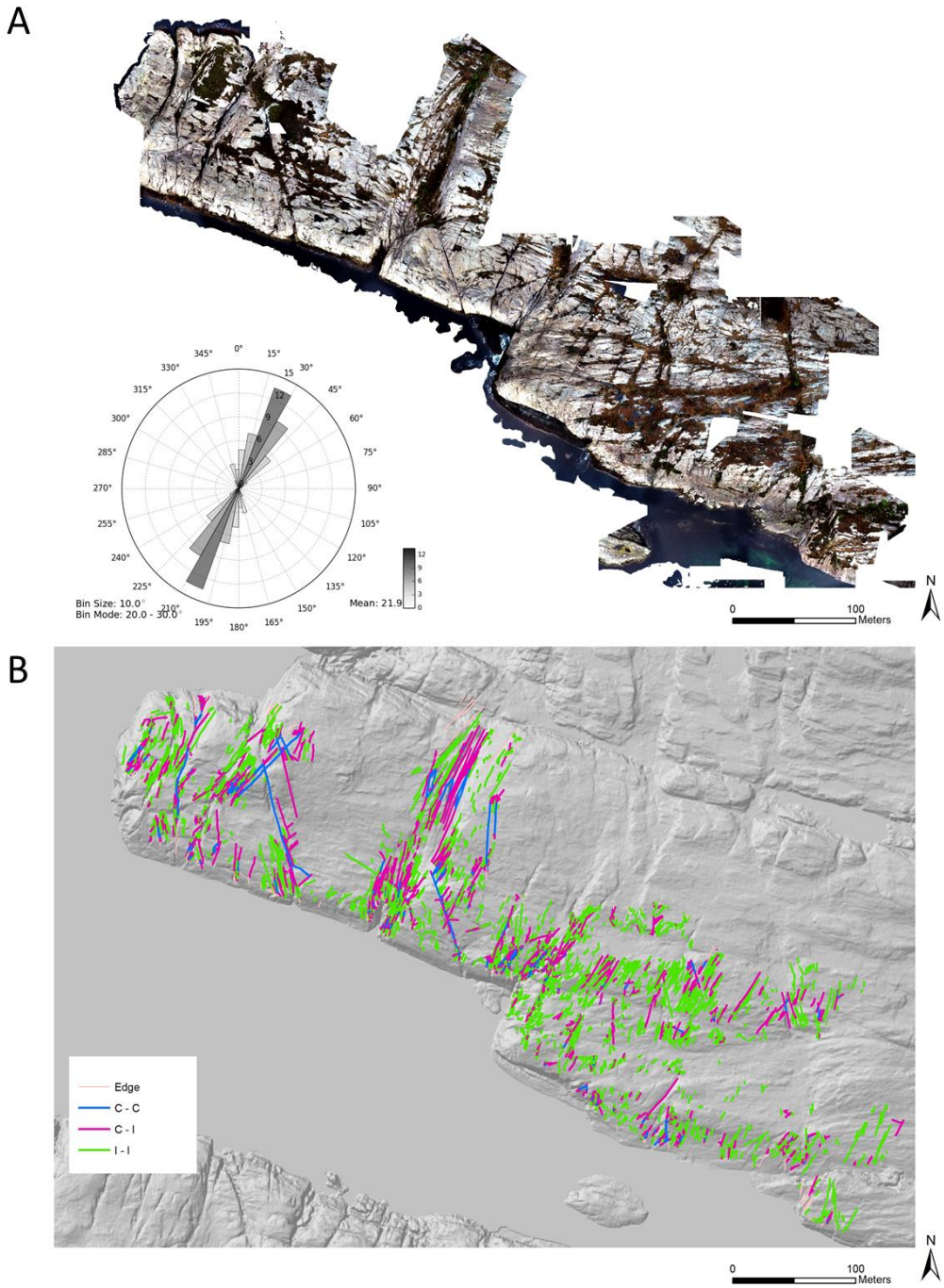


**Figure 5.2-8 A) UAV image of field location Nesvika and length weighted rose diagram based on the digitzed fractures B) Extracted branches from the digitized fractures. Color coded by branch classification. Edge are those branches that intersected the interpretation boundary, C) Ternary diagramshowing the proportion of nodes (IYX) and branches (C-I, C-C, I-I), with indications of connections per branch**

### 5.2.5 Topology

Topology (the spatial arrangement of fractures and their relation to one another) of the fracture network in Nesvika and Viksøy was analysed based on manual digitization of fractures in ArcGIS by using the Network GT toolbox (see chapter 4.2). This has resulted in a description of the arrangement of geometrical and topological parameters, and in a quantitative measure of the connectivity of the network by estimating the dimensionless connections per branch ($C_B$) (Sanderson and Nixon, 2015).

**Nesvika**

Based on a UAV image that covers c. 0,1 $km^2$ of the Nesvika location, approximately 5800 fractures were mapped in ArcGIS. The distribution of fracture orientations and trace lengths in the digitized network compares well to what was mapped by field observations. Topological parameters such as nodes, branches and connections per branch were extracted using the Network GT toolbox (Nyberg et al., 2018), and are presented in Figure 5.2-8. As seen from the ternary diagram, the network in Nesvika mainly consists of isolated nodes (I-nodes), approximately 90%, with Y-nodes as second most important. As a branch is bounded by two nodes, I-I branches (isolated-isolated) branches dominate in Nesvika, possibly reflecting the homogeneous fracture orientations as described in section 5.2.1 Because of the proportion of isolated branches, the estimated connectivity, indicated within the ternary diagram, of the network is low (below 1). However, the density map that illustrates the spatial variability of $C_B$, show that the connectivity varies throughout the network, reflecting the distribution of connected fractures.

The highest values of connections per branch are found within, and close to fracture corridors, and follow the long axis of the corridors. Because of the homogeneous orientation recorded from corridors in Nesvika and the proportion of I- and Y-nodes, the increased connectivity is most likely a result of segmented or splaying fractures. Between the zones of higher connectivity large areas of very low connectivity occur, which indicate that the network would have an anisotropic fluid flow direction.

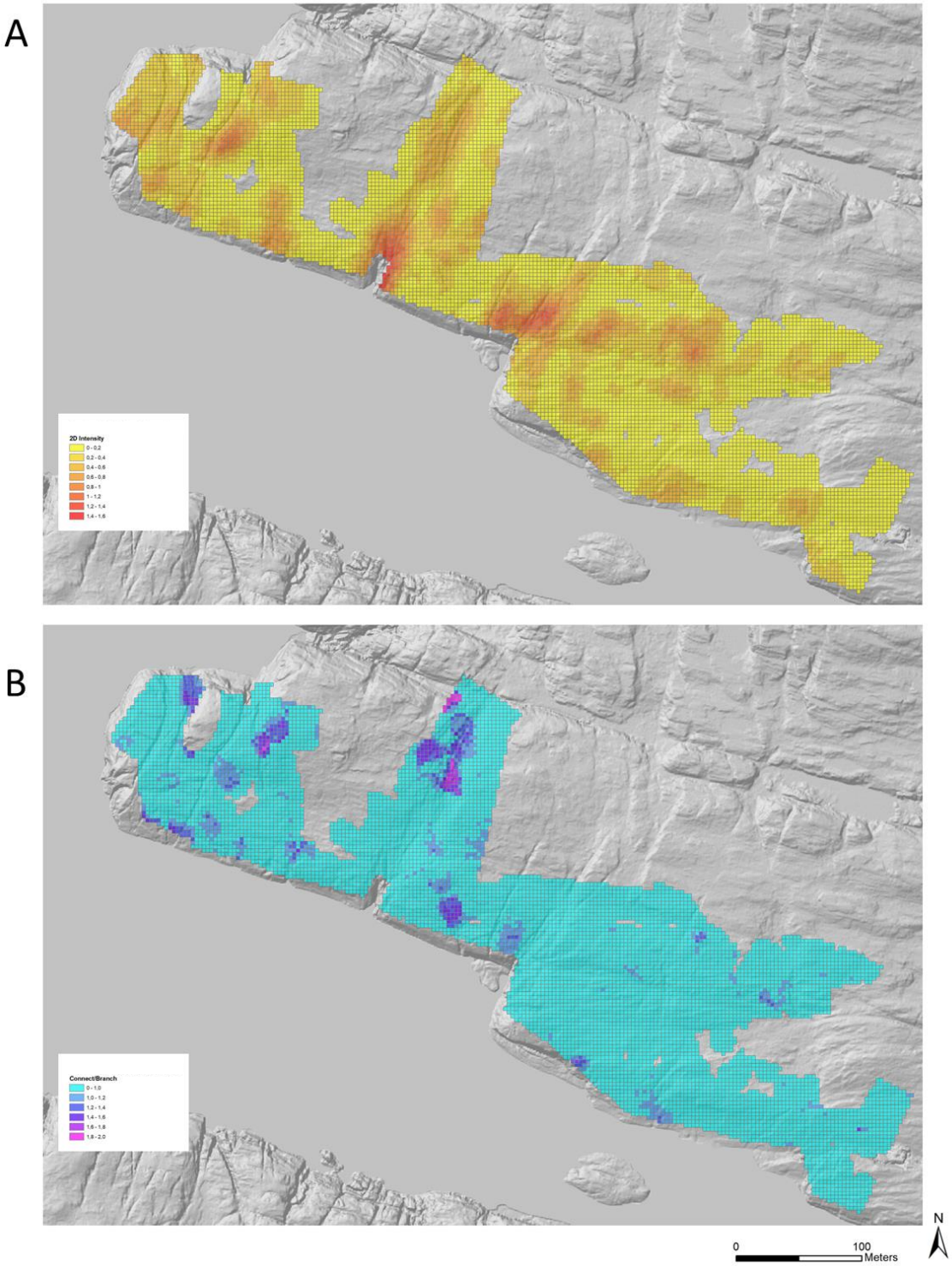


**Figure 5.2-9 Density maps created in ArcGIS by the Network GT toolbox. A) Map of 2D intensity as described in text. Red marks area of higher intensity,while yellow areasshow lower fracture intensity B) Map of connections per branch which indicates the connectivity of the network. Purple areas show the highest values of connections per branch, while blue areas show lower values.**

**Viksøy**

The high resolution UAV image covering an area of c. 16000 $m^2$ used to digitize the fracture network on Viksøy is shown in Figure 5.2-10 A, while Figure 5.2-10 B presents the extracted branches representing the 9000 manually digitized fractures on same scale as A. Fracture orientations extracted from digitized network compares well to what was mapped by field observations, showing a dominating fracture set trending NW-SE. Trace length extracted from the digitized fractures show that the majority of fractures are shorter than 2m, similar to the distribution derived by field measurements. The digitized fracture network also reveal that the fractures within corridors on Viksøy were on average shorter than the mapped fractures in the background.

Proportions of different types of nodes and branches were extracted and are plotted in ternary diagrams in Figure 5.2-10. Similar to the network in Nesvika, I- and Y-nodes were most abundant. However, the network on Viksøy had a higher fraction of C-C (connected – connected) and C-I (connected – isolated) branches, hence a slightly higher connectivity of c. 1,1 was recorded. The density map in Figure 5.2-11 illustrate how the connections per branch, which reflect the frequency of crossing fractures, vary through the fracture network. Frequency of connecting nodes is higher within and close to the corridor in the eastern part of the outcrop. This fracture corridor have, by field observations been interpreted as a sinistral strike slip fault Bastesen (in prep).

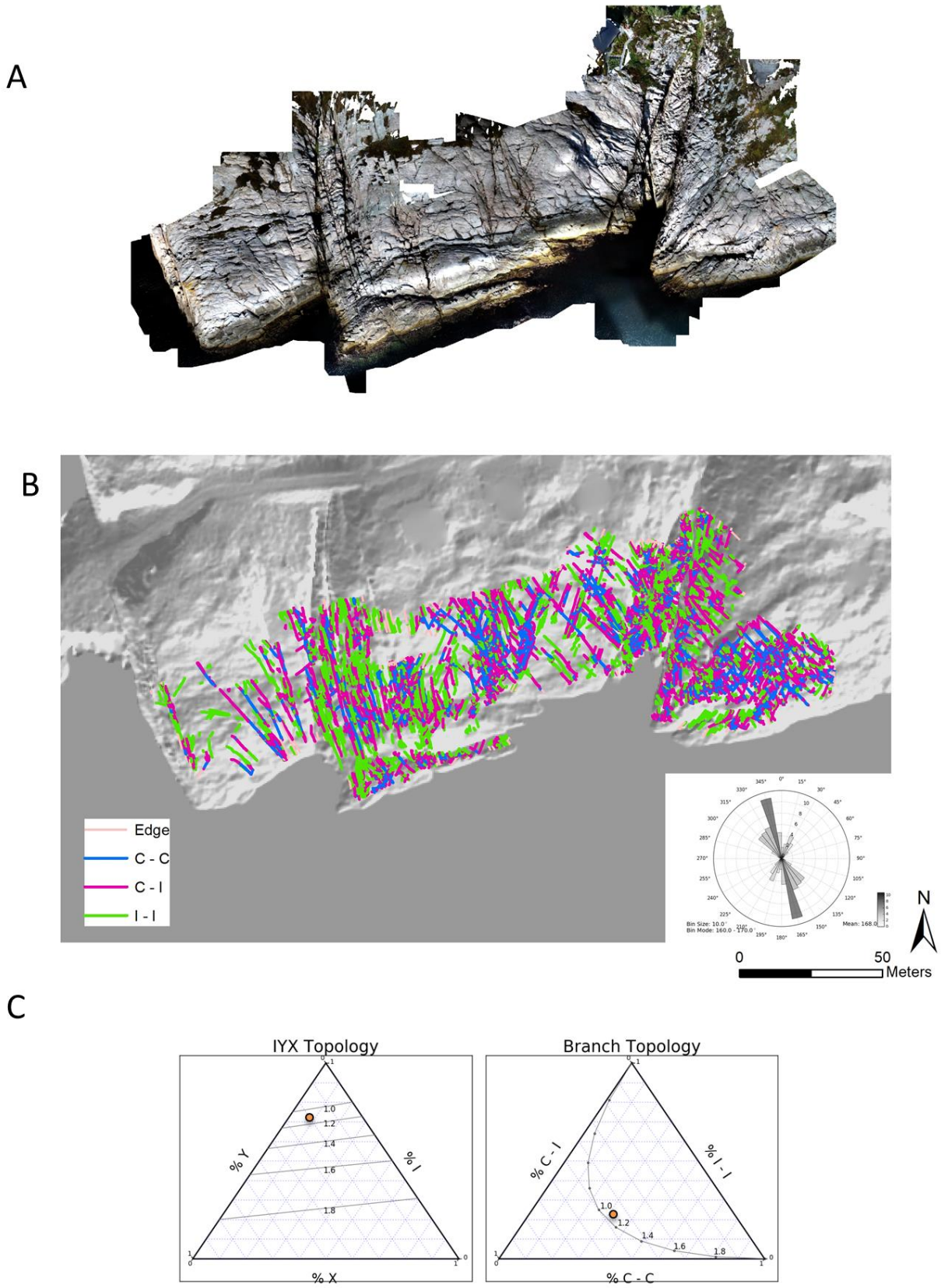


**Figure 5.2-10 A) UAV image of field location Viksøy on the same scale as B) that show the extracted branchee based on the manually digitized fractures and a length weighted rose diagram C) Ternary diagram illustrating the proportions of different types of nodes (IYX) and branches (C-I, C-C, I-I).**

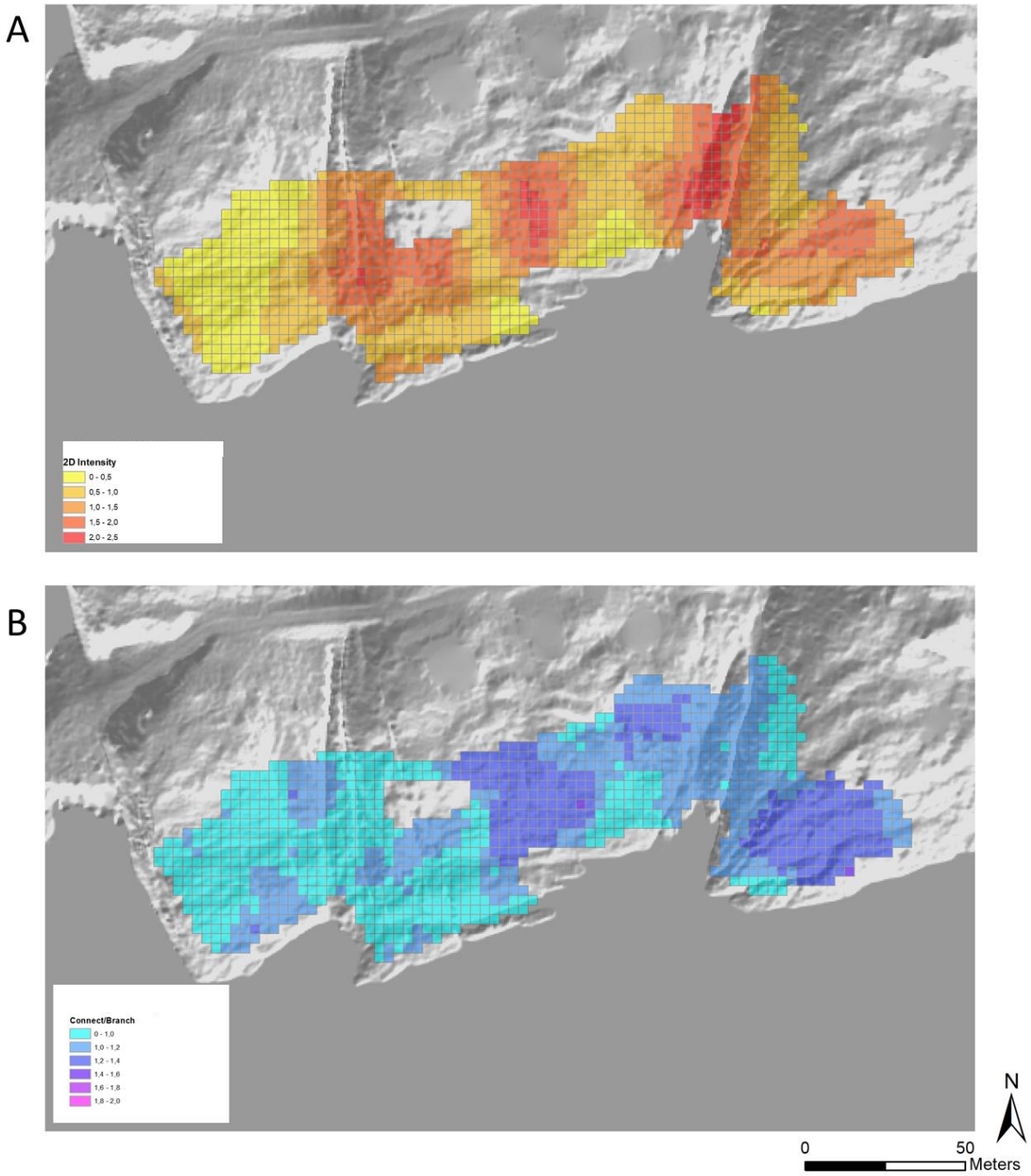


**Figure 5.2-11 Density maps created in ArcGIS with the Network GT toolbox A) illustrating the spatial variability og fracture intensity- Red indicates the highest fracture intensity, while yellow indicates lower intensity. Notice how the fracture intensity does not change as abruptly as seen in Nesvika. Image is on same scale as B. B) Connections per branch density map reflecting areas of higher and lower connectivity. Areas of high fracture intensity is not necessarily the area with highest value of connections.**

# 6 DISCUSSION

The field observations and data presented in chapter 6 will in this chapter be analysed and discussed in order to provide insight on the spatial arrangement in fracture corridors in basement rocks, to broaden the knowledge of how fracture corridors might affect fluid flow in potential basement reservoirs (e.g. hydrocarbon, groundwater, geothermal energy). The first sections address the intrinsic architecture of fracture corridors and the basis of detecting and defining them. Furthermore, several models for the development of fracture corridors will be presented. Finally, the implications of fracture corridors on fluid flow are discussed as possible analogues to subsurface reservoirs, such as basement geothermal and hydrocarbon reservoirs.

## 6.1 Fracture corridors geometry

The analysed fracture corridors created negative topographic expressions and consisted of steep, sub-parallel fractures (parallel to the strike of the corridor, NE-SW). Two fracture orientations commonly occurred, the dominating NE-SW as mentioned, and a minor NW-SE trending fracture set. These orientations correspond to the regional lineament trend on Sotra, which creates conjugate networks of fracture sets and faults. Previous studies have constrained these fracture sets to post-Caledonian extension from the onset of brittle deformation in Mid-Devonian (Larsen et al., 2003).

In the current study a range of common features of the fracture corridors were detected:

I) The outer boundary of the fracture corridors were often characterised by en echelon fracture arrangements with a slight deviated angle to the main lineament (10-30 degrees to the fracture corridor).
II) With increasing distance from the centre of the corridor a larger distribution of fracture orientations became more common, i.e. the central part had a more homogeneous fracture orientation distribution.
III) A wide range of fracture intensity and clustering was recorded, which varied most significantly across the strike of the corridors, although variations along strike was also observed.

Within fracture corridors, the highest fracture intensities were recorded at the Straume and Golta locations. The Viksøy location attested significantly higher fracture intensity compared to the other background samples. Secondary mineralization and hydrothermal alteration

commonly occurred at these three field sites, both within and outside fracture corridors. Shear fractures and slickenlines were observed in some of the fracture corridors on the Golta location, indicating shear displacement. Scanlines sampled close to a fault or in corridors with shear displacement indications, recorded higher fracture frequencies. This can be illustrated by the two scanlines Golta D and E, which were positioned within the same fracture corridor. The Golta D scanline was positioned closer to a previously interpreted fault and displayed a much higher fracture frequency than the Golta E scanline, which was more distant to the fault. Furthermore, the Viksøy scanline was sampled amidst two corridors, on that has been interpreted as a strike slip fault (Bastesen in prep). This could explain the considerably higher background frequency sampled on Viksøy compared to the other field locations. The observations described above, indicate that the fracture corridors on Golta, Starume and Viksøy can be classified as faults, and fracture corridors where fracture frequency is high but no horizontal or vertical displacement could be detected.

Nesvika stand out from the other localities by showing generally lower fracture intensity, consisting of mostly mode I fractures (opening mode), showing no detectable vertical or horizontal displacement and almost absent secondary mineralization or alteration, based on these observations the fracture corridors in Nesvika are interpreted as joint swarms.

The spatial arrangement (fracture orientations, length, distribution) of the investigated fracture corridors on Sotra was similar to what was mapped for corridors in basement rocks in Sunnfjord (Braathen and Gabrielsen, 1998; Gabrielsen and Braathen, 2014). These studies identified a zonational architecture divided the fracture corridors into sub-zones characterised by fracture types, -intensity, orientation, presence of fault rock, secondary mineralisation and/or clay (as further described in chapter 2.2). Following the classification by Braathen and Gabrielsen, Nesvika mainly consist of the distal sub-zones and qualify as a joint swarm. While the more complex patterns observed at the other field sites, Golta, Straume and Viksøy can be ascribed to faults and fracture corridors comprising more of the central sub-zones reflecting larger strain accumulation.

The architecture observed in this study is based on one-dimensional linear scanlines complemented by 2D mapping of orthophotos. This mapping technique provides a better foundation to describe length, intrinsic geometry and clustering, in addition to a reduced bias related to undersampling of fracture sets as the linear scanline is prone to (Terzaghi, 1965).

Linear scanlines are known to provide an orientation bias by undersampling fracture sets with low angle to the scanline (Terzaghi, 1965), which has been corrected for.

## 6.2 Definition of fracture corridors

A fracture corridor is commonly defined as a narrow zone of enhanced fracture intensity, but a more precise or quantitative definition of characteristic fracture intensity is lacking. The detailed mapping conducted in this study show that the fracture intensity varies, not only from one corridor to another, but also within short distances in the same corridor. Furthermore, the background areas (outside corridors) at one locality recorded higher fracture intensities than fracture corridors at other localities. Thus, the results of this study support the observations by Sanderson and Peacock (2019), suggesting that the absolute value of fracture intensity is not suited to establish a quantitative measure for defining fracture corridors.

The ratio of fracture intensity in a corridor to the background is inferred to be a better way of examining ways to define characteristic fracture intensities found in fracture corridors. However, as discussed by Sanderson and Peacock (2019), it is challenging to determine the fracture intensity outside the corridor when the spatial extent of the corridor is not defined. Previous studies have suggested that the boundary of a fracture corridor is based on geometric properties (fracture intensity, fracture geometry orientation) (sensu, Braathen and Gabrielsen, 1998; Gabrielsen and Braathen, 2014). Background samples collected during this project was sampled from areas outside the topographic expression of the interpreted fracture corridors. On average the fracture corridors assessed in this study had fracture frequencies between three to six times higher than the background area. Following the methods proposed by Sanderson and Peacock (2019) a fracture corridor may be detected using a threshold of two times the uniform intensity for sequences comprising more than 5% of the fractures.

However, the methods suggested by Sanderson and Peacock (2019) was recommended for samples of parallel to sub-parallel fractures. Thus, the more complex, stair-stepped curve in the cumulative frequency plots presented in chapter 5.2 could be explained by the wider distribution of fracture orientations observed in this study. Furthermore, fracture clusters were also observed in the background, utilizing the ad hoc threshold (two times the intensity of the uniform distribution for 5% of the fractures) for a fracture corridor as suggested by Sanderson and Peacock (2019), some of these clusters could qualify as fracture corridors although their

topographic expression is minimal. The observations by Gabrielsen and Braathen (2014) indicated that a threshold of 1 f/m over a distance of 35m could be used to limit the extent of a fracture corridor. This compares well with the value of background fracture frequency sampled in this study (an average 1 f/m from all background scanlines). The statistical analyses proposed by Sanderson and Peacock (2019) were limited to sub-parallel fractures. Thus, the fracture database from this study, which is based on all fracture sets (various orientations and attributes) was not analysed further following their methodology. However, the database from this study could be utilized in these analyses in future work.

Since only a few of the many fracture corridors on Sotra were analysed through this study, more research in this area will be needed to prepare a more robust database for a regional scale analysis of fracture corridors. The detailed mapping of fracture intensity and spatial variation of geometric and topological properties contribute to a broader knowledge of the spatial arrangement within fracture corridors. Thus, the work of this study provide quantified measures that, complemented by further research and field observations, could contribute to the establishment of a more quantitative definition of fracture corridors.

## 6.3 Fracture corridor development

Joint spacing in sedimentary sequences is generally found to be proportional to the thickness of the deformed layer (Pollard and Aydin, 1988). Explaining the narrow spacing observed in fracture swarms and corridors has thus been challenging (Olson, 2004). The study by Olson (2004) found that the mechanical properties of the rock (more specifically the subcritical index), is important for the development of fracture swarms and corridors. Souque et al. (2019) further emphasized the impact of the structural history and pre-existing faults for fracture corridor development. The majority of studies on fracture corridor development has focused on sedimentary rocks (e.g. Olson, 2004; Ogata et al., 2014; Stephenson et al., 2007; Souque et al., 2019). How fracture corridors develop in crystalline rocks on the other hand, has received less attention (Braathen and Gabrielsen, 1998, Gabrielsen and Braathen, 2014).

From the Zagros Mountains, fold-related development of fracture corridors in bedded carbonates has been recognized (Stephenson et al., 2007). Furthermore, Ogata et al. (2014) also identified fold-related fracture corridors in outcrops in Utah. Both studies showed that fracture corridors developed in the crestal area of anticlines, as seen in Figure 6.3-1, and

flexural slip is believed to impact the development. Similar to observations from Sotra, a wider distribution of fracture orientations occurred with distance from the centre of the corridor which mainly consisted of lineament parallel fractures (Stephenson et al., 2007). Post-Caledonian large-scale folding has been identified in the Øygarden Complex on Sotra creating the E-W and N-S trending antiforms, (Larsen et al., 2003). E-W to NE-SW trending semi-brittle faults (set Ia) were by Larsen et al. (2003) interpreted as a result of local strain related to the development of E-W trending folds. However, fracture corridors are common features on Sotra, not just in the crestal areas of these large-scale folds. Thus, a fold-related development appears to be a less likely explanation for the fracture corridors on Sotra.

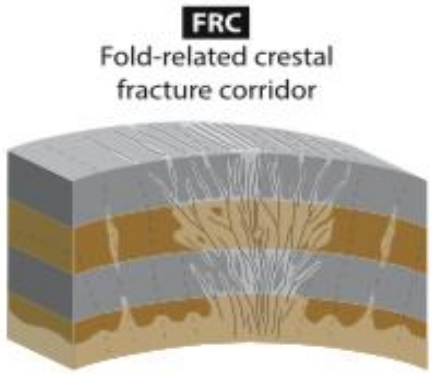


**Figure 6.3-1 Conceptual model for fold-related fracture corridors. From Ogata et al. (2014)**

The fracture corridors analysed by Souque et al. (2019) were geometrically linked to faults, either by abutting against the fault with an oblique angle, or by containing a fault sub-parallel to the corridor. Based on these observations a model for fracture corridor development caused by stress concentrations at steps, bend, tips or fault intersections and fault reactivation was proposed. The pattern of spatially associated faults and fracture corridors differentiates from the observations on Sotra as faults and fracture corridors on Sotra showed crosscutting relationships, while other corridors appeared to be isolated. As discussed by Souque et al. (2019), fracture corridors may seem isolated because the nucleation point from a fault is not coincident with the outcrop. However, no crosscutting relationships between faults and fracture corridors were detected by Souque et al. (2019).

Previous studies of fracture corridors in crystalline rocks suggested a zonational architecture ascribed to differences in strain accumulation (Braathen and Gabrielsen, 1998; Gabrielsen and Braathen, 2014). In sedimentary rocks faults are often associated with a zone of shear deformation (e.g. deformation bands) in the fault tip process zone (Figure 6.3-2). Braathen and Gabrielsen (1998) interpreted the en echelon fracture pattern (a pattern commonly associated with shear) in joint swarms and distal parts of fracture corridors, to be the equivalent fault tip process zone deformation in crystalline rocks. Thus, joint swarms can be regarded as surface expressions of faults and could prograde into fracture corridors, and faults with increased strain (Braathen and Gabrielsen, 1998; Gabrielsen and Braathen, 2014). Similar intrinsic architecture was found in the fracture corridors on Sotra in this study. Similar mechanisms could thus be a potential model for the development of fracture corridors in basement rocks on Sotra.

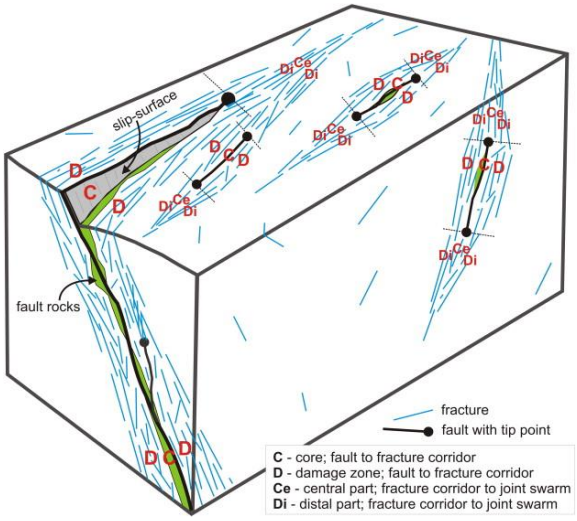


**Figure 6.3-2 Model showing the relationship between joint swarms, fracture corridors and faults by Gabrielsen and Braathen (2014).**

## 6.3.1 Fracture corridor development on Sotra

Fracture corridors on Sotra are parallel to sub-parallel to the NE-SW trending Devonian set I fracture orientation and to the NW-SE trending Permo-Triassic set of dykes and normal faults. These faults show cohesive fault rocks, deformation related to the brittle-ductile transition (shear zones), hydrothermal mineralization and alteration. The fracture corridors on the other

hand, do not contain cohesive fault rocks or ductile deformation, but most, except the joint swarms in Nesvika, contained hydrothermal mineralization and alteration. The occurrence of epidote, which has been ascribed to Devonian fracturing and development of set I fractures by Larsen et al. (2003), in fractures within the investigated fracture corridors indicate that the fracture corridors initiated during set I fracturing by NW-SE extension. However, epidote was absent within many of joints present in the corridors and totally absent within the swarms in Nesvika. Could these features be ascribed to reactivation of older, Post-Caledonian fracture sets? Exact timing for the development of the fracture corridors are impossible without dating or good cross relations with known features, such as the Permo-Triassic dykes or dating of alteration (Fossen, 1998).

## 6.4 Fracture corridors significance for fluid flow

The spatial distribution of fractures and topological parameters has been analysed and quantified for two different fracture networks. Joint swarms in Nesvika, showed no detectable horizontal or vertical displacement, and mainly consisted of parallel to sub-parallel fractures, creating a fracture network with low connectivity. While the fracture network on Viksøy, containing a previously interpreted strike slip fault (Bastesen, in prep), generally comprised a higher fracture intensity and wider distribution of fracture orientations. The higher fracture intensity and a variety of orientations resulted in a more connected fracture network (based on connections per branch) than in Nesvika, especially in the proximity of the strike slip fault, where the fractures had longer trace lengths than in the fault core.

Faults and fractures are the main conduits for fluid flow in tight rocks, such as crystalline and metamorphic basement (Nelson, 2001). Several authors have previously described the importance of fracture corridors in fluid flow in subsurface reservoirs (e.g. Braathen and Gabrielsen, 1998; Ozkaya, 2006, Questiaux et al., 2010; Ogata et al., 2014; Gabrielsen and Braathen, 2014; Ozkaya, 2019; Souque et al., 2019). Fracture corridors could be problematic zones in reservoirs because of their potential role in causing early water break through in hydrocarbon reservoirs (Ozkaya, 2019; Souque 2019), compromising top seal capacity (Ogata et al., 2014), which are some of the reasons fracture corridors and their distribution of conductive fractures are important to understand and detect in subsurface reservoirs.

Fracture corridors are common features in the basement rocks on Sotra. The abundance and their continuous lengths, up to several kilometres, indicate that fracture corridors could be significant fluid flow conduits in subsurface basement reservoirs. Many of the observed fracture corridors were not visibly related to shear deformation and contained no fault rocks or gouge (clay). Along with the fracture frequency within the corridors (0,97-5,83 f/m) in contrast to the lower frequency in the background (0,33-2,26 f/m), the absence of fault rocks, gouge indicate that fracture corridors in basement reservoirs could provide a high along strike permeability. The fracture corridors could also create a vertical migration path for fluids (Questiaux et al., 2010, Ozkaya, 2019). Thus, understanding the distribution of conductive fractures in basement reservoirs is important as they control the porosity and permeability (Nelson, 2001). Although fracture corridors are continuous features, the fracture distribution is difficult to detect by seismic, as the rapid change in fracture intensity and the width/length of the corridor is below the seismic resolution or show no detectable offset (Questiaux et al., 2010). This study contributes to a broader knowledge of the spatial arrangement in fracture corridors in a possible field analogue to the basement on the Norwegian continental shelf. The quantified geometric and topological parameters can be utilized in geological and fluid flow models and contribute to better predict reservoir behaviour.

# 7 CONCLUSIONS

## 7.1 Conclusions

The aim of this study was to broaden the knowledge of the spatial architecture in fracture corridors by characterizing the geometry and topology of the fracture network, and thus improve the understanding of how fracture corridors might affect fluid flow in hydrocarbon-, geothermal- and groundwater basement reservoirs From the results and discussion presented, the following conclusions are drawn:

- The fracture corridors mainly consist of clustered, sub-parallel fractures, parallel to the main strike of the lineament. They have an increased fracture frequency up to 6 times higher than the background, and the fracture frequency drops rapidly with increasing distance from the centre of the corridors.
- The topology of the fracture corridors is characterized by isolated branches, and thus, a low connectivity and a potential anisotropic fluid flow direction. However, the fracture corridors are characterised by absence of fault rocks and gouge which could act as barriers or baffles to fluid flow, thus they are potential high-permeable structures.
- Polyphase deformation and formation of fracture corridors is indicated by different fracturing modes, it is therefore challenging to constrain the development of fracture corridors on Sotra to distinct deformation phases based on the observations from this study.

By quantification geometric and topological parameters, as conducted in this study, spatial arrangements within different fracture networks can be compared. Thus, the findings of this study provide measures that can be used to establish a quantitative definition applicable to identify and detect fracture corridors. Fracture corridors are often below the seismic resolution and are thus not detected by seismic prospecting. Basement plays are poorly constrained by seismic, thus, outcrop studies, as this study, are valuable sources of information since fractures are the main conduits for fluid flow in basement reservoirs. The results of this study contribute to the understanding of the spatial arrangement of fracture corridors in crystalline rocks as few outcrop-based studies have been conducted.

## 7.2 Suggestions for further work

This study provides a documentation and quantification of the geometric and topological parameters characterizing the spatial arrangement of the observed fracture corridors. Complementing the database from this study with observations from more fracture corridors and further investigate the statistical basis for identification and detection of fracture corridors, following Sanderson and Peacock (2019), would provide valuable information.

The hydrocarbon reservoir discovery Rolvsnes was found in altered and fractured basement rocks. It would therefore be interesting to conduct a thin section analysis and investigate the geochemical alteration observed in the fracture corridors. Indications of weathering was during this project only observed within fractures in the Straume location by the occasional presence of clay, but it would be interesting to see if similar alteration and weathering as in the Rolvsnes field could be detected by thin section analysis or geophysical data.

Furthermore, it would be of interest to perform a simplified discrete fracture network modelling using the database from this study to further evaluate fluid flow properties such as permeability, permeability anisotropy and -enhancement as a function of distance away from the fracture corridors.

# 8 REFERENCES


Andersen, T. B., & Jamtveit, B. (1990). Uplift of deep crust during orogenic extensional collapse: A model based on field studies in the Sogn-Sunnfjord Region of western Norway. *Tectonics*, *9*(5), 1097-1111.

Andersen, T. B., Jamtveit, B., Dewey, J. F., & Swensson, E. (1991). Subduction and eduction of continental crust: major mechanisms during continent-continent collision and orogenic extensional collapse, a model based on the south Norwegian Caledonides. *Terra Nova*, *3*(3), 303-310.

Bastesen, E. (2019). Manuscript in preparation.

Belaidi, A., Bonter, D., Slightam, C., & Trice, R. (2018). The Lancaster Field: Progress in opening the UK's fractured basement play. *Geological Society, London, Petroleum Geology Conference Series*, 8(1), 385-398.

Bering, D.H. (1984*). Tektonometamorf Utvikling Av Øygarden Gneiskompleks I Sund, Sotra*. (Cand. Real.). University of Bergen.

Berkowitz, B., Bour, O., Davy, P., & Odling, N. (2000). Scaling of fracture connectivity in geological formations. *Geophysical Research Letters*, *27*(14), 2061-2064.

Bingen, B., Nordgulen, Ø., & Viola, G. (2008). A four-phase model for the Sveconorwegian orogeny, SW Scandinavia. *Norwegian Journal of Geology/Norsk Geologisk Forening*, *88*(1).

Bingen, B., Skår, Ø., Marker, M., Sigmond, E. M., Nordgulen, Ø., Ragnhildstveit, J., Mansfeld, J., Tucker, R.D., & Liégeois, J. P. (2005). Timing of continental building in the Sveconorwegian orogen, SW Scandinavia. *Norwegian Journal of Geology*, *85, 87-116.*

Bogdanova, S. V., Bingen, B., Gorbatschev, R., Kheraskova, T. N., Kozlov, V. I., Puchkov, V. N., & Volozh, Y. A. (2008). The East European Craton (Baltica) before and during the assembly of Rodinia. *Precambrian Research*, *160*(1-2), 23-45.

Boundy, T. M., Essene, E. J., Hall, C. M., Austrheim, H., & Halliday, A. N. (1996). Rapid exhumation of lower crust during continent-continent collision and late extension:

Evidence from 40Ar/39Ar incremental heating of hornblendes and muscovites, Caledonian orogen, western Norway. *Geological Society of America Bulletin*, *108*(11), 1425-1437.

Braathen, A., & Gabrielsen, R. H. (1998*).* Lineament architecture and fracture distribution in metamorphic and sedimentary rocks, with application to Norway. Geological Survey of Norway Report, 98 (043), 78.

Caine, J. S., Evans, J. P., & Forster, C. B. (1996). Fault zone architecture and permeability structure. *Geology*, *24*(11), 1025-1028.

Cawood, P. A., & Pisarevsky, S. A. (2017). Laurentia-Baltica-Amazonia relations during Rodinia assembly. *Precambrian Research*, *292*, 386-397.

Corfu, F., Andersen, T.B. & Gasser, D., 2014. The Scandinavian Caledonides: main features, conceptual advances and critical questions. *Geological Society, London, Special Publications*, 390(1), 9–43.

Fossen, H. (1992). The role of extensional tectonics in the Caledonides of south Norway. *Journal of structural geology*, *14*(8-9), 1033-1046.

Fossen, H. (1998). Advances in understanding the post-Caledonian structural evolution of the Bergen area, West Norway. *Norsk Geologisk Tidsskrift*, *78*(1), 33-46.

Fossen, H. (2000). Extensional tectonics in the Caledonides: Synorogenic or postorogenic?. *Tectonics*, *19*(2), 213-224.

Fossen, H. (2010). *Structural Geology*. Cambridge: Cambridge University Press.

Fossen, H., & Dunlap, W. J. (1998). Timing and kinematics of Caledonian thrusting and extensional collapse, southern Norway: evidence from 40Ar/39Ar thermochronology. *Journal of structural geology*, *20*(6), 765-781.

Fossen, H., & Dunlap, W.J. (2006). Age constraints on the late Caledonian (Scandian) deformation in the Major Bergen Arc, SW Norway. *Norwegian Journal of Geology*, *86*(1), 59-70

Fossen, H., & Rykkelid, E. (1990). Shear zone structures in the Øygarden area, West Norway. *Tectonophysics*, *174*(3-4), 385-397.

Fossen, H., & Rykkelid, E. (1992a). The interaction between oblique and layer-parallel shear in high-strain zones: observations and experiments. *Tectonophysics*, *207*(3-4), 331-343.

Fossen, H., & Rykkelid, E. (1992b). Postcollisional extension of the Caledonide orogen in Scandinavia: Structural expressions and tectonic significance. *Geology*, *20*(8), 737-740.

Gabrielsen, R. H., & Braathen, A. (2014). Models of fracture lineaments—Joint swarms, fracture corridors and faults in crystalline rocks, and their genetic relations. *Tectonophysics*, *628*, 26-44.

Gabrielsen, R. H., Braathen, A., Dehls, J., & Roberts, D. (2002). Tectonic lineaments of Norway. *Norsk Geologisk Tidsskrift*, *82*(3), 153-174.

Gee, D. G., Fossen, H., Henriksen, N., & Higgins, A. K. (2008). From the early Paleozoic platforms of Baltica and Laurentia to the Caledonide Orogen of Scandinavia and Greenland. *Episodes*, *31*(1), 44-51.

Gutmanis, J. (2009, January). Basement reservoirs-a review of their geological and production characteristics. In *International Petroleum Technology Conference*. International Petroleum Technology Conference.

Hudson, J. A., & Priest, S. D. (1983). Discontinuity frequency in rock masses. *International Journal of Rock Mechanics and Mining Sciences & Geomechanics Abstracts*, 20 (2), 73-89.

Koning, T. (2003). Oil and gas production from basement reservoirs: examples from Indonesia, USA and Venezuela. *Geological Society, London, Special Publications*, *214*(1), 83-92.

Ksienzyk, A. K., Dunkl, I., Jacobs, J., Fossen, H., & Kohlmann, F. (2014). From orogen to passive margin: constraints from fission track and (U–Th)/He analyses on Mesozoic uplift and fault reactivation in SW Norway. *Geological Society, London, Special Publications*, *390*(1), 679-702.

Larsen, Ø., Fossen, H., Langeland, K., & Pedersen, R. B. (2003). Kinematics and timing of polyphase post-Caledonian deformation in the Bergen area, SW Norway. *Norwegian Journal of Geology*, *83*(3), 149-165.

Laubach, S. E., Lamarche, J., Gauthier, B. D., Dunne, W. M., & Sanderson, D. J. (2018). Spatial arrangement of faults and opening-mode fractures. *Journal of Structural Geology*, *108*, 2-15.

Manzocchi, T. (2002). The connectivity of two-dimensional networks of spatially correlated fractures. *Water Resources Research*, *38*(9), 1-1-1-20.

McNamara, D., Faulkner, D., & McCarney, E. (2014). Rock properties of Greywacke Basement hosting geothermal reservoirs, New Zealand: Preliminary results. In Proceedings Thirty-ninth Workshop on Geothermal Reservoir Engineering, SGP-TR-202

Nelson, R. (1985). *Geologic analysis of naturally fractured reservoirs*. Gulf Publishing, Houston, TX.

Nelson, R. (2001). *Geologic Analysis of Naturally Fractured Reservoirs* (2nd ed.). Burlington: Elsevier Science.

Nielsen, S. B., Gallagher, K., Leighton, C., Balling, N., Svenningsen, L., Jacobsen, B. H., Thomsen, E., Nielsen, O. B., Heilmann-Clausen, C., Egholm, D. L., Summerfield, M.A., Clausen, O. R., Piotrowski, J. A., Thorsen, M., R., Huuse, M., Abrahamsen, N., King, C. & Lykke-Andersen, H. (2009). The evolution of western Scandinavian topography: a review of Neogene uplift versus the ICE (isostasy–climate–erosion) hypothesis. *Journal of Geodynamics*, *47*(2-3), 72-95.

Nyberg, B., Nixon, C. W., & Sanderson, D. J. (2018). NetworkGT: A GIS tool for geometric and topological analysis of two-dimensional fracture networks. *Geosphere*, *14*(4), 1618-1634.

Ogata, K., Senger, K., Braathen, A., & Tveranger, J. (2014). Fracture corridors as seal-bypass systems in siliciclastic reservoir-cap rock successions: Field-based insights from the Jurassic Entrada Formation (SE Utah, USA). *Journal of Structural Geology*, *66*, 162-187.

Olson, J. E. (2004). Predicting fracture swarms. The influence of subcritical crack growth and the crack-tip process zone on joint spacing in rock. *Geological Society, London, Special Publications*, *231*(1), 73-88.

Ozkaya, S. (2019). Fracture modeling from borehole image logs and water invasion in carbonate reservoirs with layer-bound fractures and fracture corridors. *Journal of Petroleum Science and Engineering*, *179*, 199-209.

Ozkaya, S. I., & Richard, P. D. (2006). Fractured reservoir characterization using dynamic data in a carbonate field, Oman. *SPE Reservoir Evaluation & Engineering*, *9*(03), 227-238.

Peacock, D. C. P., Nixon, C. W., Rotevatn, A., Sanderson, D. J., & Zuluaga, L. F. (2016). Glossary of fault and other fracture networks. *Journal of Structural Geology*, *92*, 12-29.

Pollard, D. D., & Aydin, A. (1988). Progress in understanding jointing over the past century. *Geological Society of America Bulletin*, *100*(8), 1181-1204.

Questiaux, J. M., Couples, G., & Ruby, N. (2010). Fractured reservoirs with fracture corridors. *Geophysical Prospecting*, *58*(2), 279-295.

Riber, L., Dypvik, H., & Sørlie, R. (2015). Altered basement rocks on the Utsira High and its surroundings, Norwegian North Sea. *Norwegian Journal of Geology*, *95*(1), 57-89.

Roberts, D. (2003). The Scandinavian Caledonides: event chronology, palaeogeographic settings and likely modern analogues. *Tectonophysics*, *365*(1-4), 283-299.

Roberts, N. M., & Slagstad, T. (2015). Continental growth and reworking on the edge of the Columbia and Rodinia supercontinents; 1.86–0.9 Ga accretionary orogeny in southwest Fennoscandia. *International Geology Review*, *57*(11-12), 1582-1606.

Sanderson, D. J., & Nixon, C. W. (2015). The use of topology in fracture network characterization. *Journal of Structural Geology*, *72*, 55-66.

Sanderson, D. J., & Peacock, D. C. (2019). Line sampling of fracture swarms and corridors. *Journal of Structural Geology*, *122*, 27-37.

Scheiber, T., & Viola, G. (2018). Complex Bedrock Fracture Patterns: A Multipronged Approach to Resolve Their Evolution in Space and Time. *Tectonics*, *37*(4), 1030-1062.

Schultz, R. A., & Fossen, H. (2008). Terminology for structural discontinuities. *AAPG bulletin*, *92*(7), 853-867.

Singhal, B., & Gupta, R. (2010). *Applied Hydrogeology of Fractured Rocks (2nd ed.).*Dordrecht: Springer Netherlands.

Slagstad, T., Roberts, N. M., & Kulakov, E. (2017). Linking orogenesis across a supercontinent; the Grenvillian and Sveconorwegian margins on Rodinia. *Gondwana Research*, *44*, 109-115.

Slagstad, T., Roberts, N. M., Marker, M., Røhr, T. S., & Schiellerup, H. (2013). A non-collisional, accretionary Sveconorwegian orogen. *Terra Nova*, *25*(1), 30-37.

Souque, C., Knipe, R., Davies, R., Jones, P., Welch, M., & Lorenz, J. (2019). Fracture corridors and fault reactivation: Example from the Chalk, Isle of Thanet, Kent, England. *Journal of Structural Geology*, 122, 11-26.

Stephenson, B. J., Koopman, A., Hillgartner, H., McQuillan, H., Bourne, S., Noad, J. J., & Rawnsley, K. (2007). Structural and stratigraphic controls on fold-related fracturing in the Zagros Mountains, Iran: implications for reservoir development. *Geological Society, London, Special Publications*, *270* (1), 1.2-21

Sturt, B. A., Skarpenes, O., Ohanian, A. T., & Pringle, I. R. (1975). Reconnaissance Rb/Sr isochron study in the Bergen Arc System and regional implications. *Nature*, *253*(5493), 595-599.

Terzaghi, R. D. (1965). Sources of error in joint surveys. *Geotechnique*, *15*(3), 287-304.

Torabi, A., Alaei, B., & Ellingsen, T. (2018). Faults and fractures in basement rocks, their architecture, petrophysical and mechanical properties. *Journal of Structural Geology*, 117, 256-263.

Torsvik, T. H., & Cocks, L. R. M. (2005). Norway in space and time: A Centennial cavalcade. *Norwegian Journal of Geology, 85, 73-86*.

Trice, R. (2014). Basement exploration, West of Shetlands: progress in opening a new play on the UKCS. *Geological Society, London, Special Publications*, *397*(1), 81-105.

Van der Pluijm, B. A. & Marshak, S. (2004). *Earth structure (2nd ed.).* New York. W.W. Norton

Watkins, H., Bond, C., Healy, D., & Butler, R. (2015). Appraisal of fracture sampling methods and a new workflow to characterise heterogeneous fracture networks at outcrop. *Journal of Structural Geology*, *72*, 67-82.

Wibberley, C. A., Yielding, G., & Di Toro, G. (2008). Recent advances in the understanding of fault zone internal structure: a review. *Geological Society, London, Special Publications*, *299*(1), 5-33.

Wiest, J. D., Jacobs, J., Ksienzyk, A. K., & Fossen, H. (2018). Sveconorwegian vs. Caledonian orogenesis in the eastern Øygarden Complex, SW Norway–Geochronology, structural constraints and tectonic implications. *Precambrian Research*, *305*, 1-18.

# Appendix I – Workflow ArcGIS

1. The first step was to create a geodatabase (.gdb) where outputs from the project in ArcMap would be saved. Then the georeferenced UAV image (tiff file) of the locality was added into a blank project in ArcMap.
2. To digitize the fracture traces a polyline shapefile was created by clicking the ArcCatalog symbol, right clicking the folder where the geodatabase was located and select the option of creating a new shapefile. After activating the snapping tool, which records where different polylines intersect, the start editing option was selected by clicking the edit tool. Fractures were then digitized by drawing a polyline following the interpreted fracture traces in the UAV image, each fracture as an individual polyline.

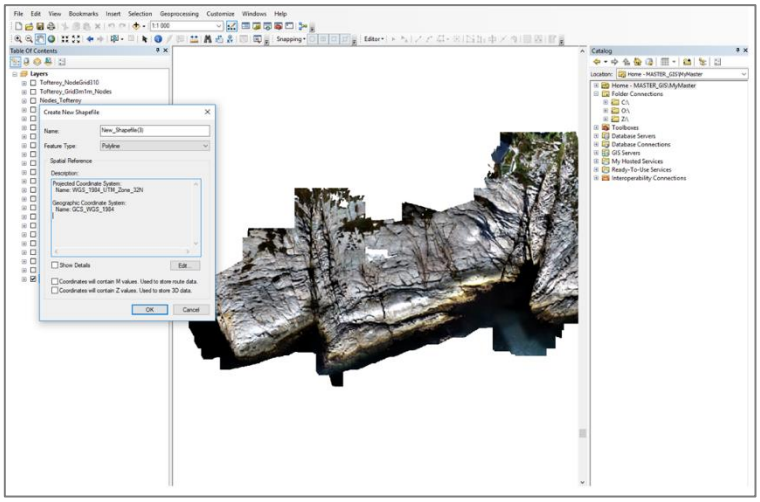

3. When the digital fracture network was created, the Network GT toolbox could be utilized. The steps for installing and applying the toolset available in the supplementary data of Nyberg et al. (2018) were followed.
4. First an interpretation boundary, that marks the extent of the sample area was made. This was conducted following the procedure in step 3, but choosing polygon instead of polyline. The polygon interpretation boundary was drawn so that fractures with trace lengths exceeding the extent of the UAV image were intersected by the interpretation boundary. Thus, when branches and nodes are extracted these will be marked with "Edge" in stead of a branch and node classification that is possibly incorrect which

would affect the interpretation of the fracture network.

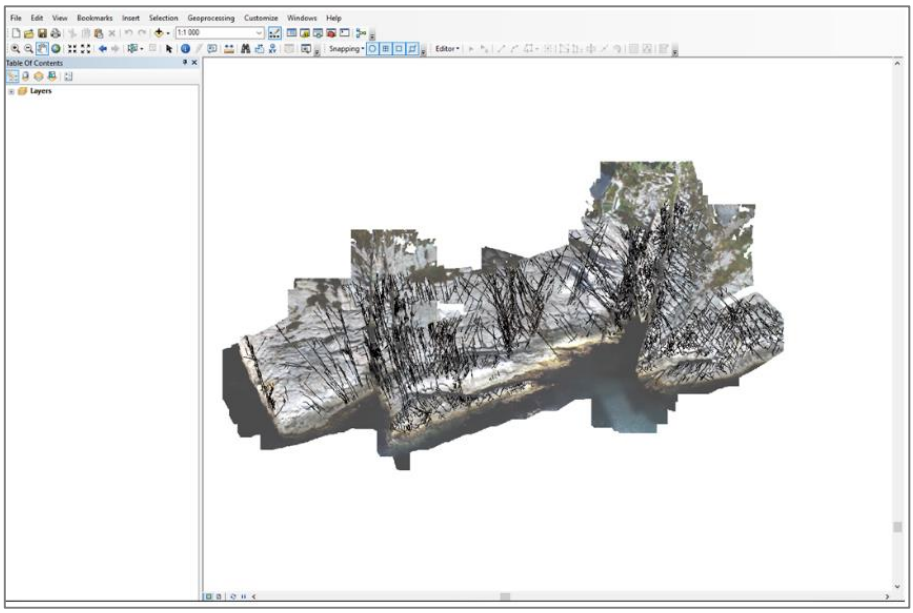

5. To map the spatial variations a grid sampling of the network was conducted. The grid was created using the '**Network Grid Sampling'** tool. Width x height of the cell and search radius was selected as 3x3m and 10m, respectively, and the previously created interpretation boundary as input.

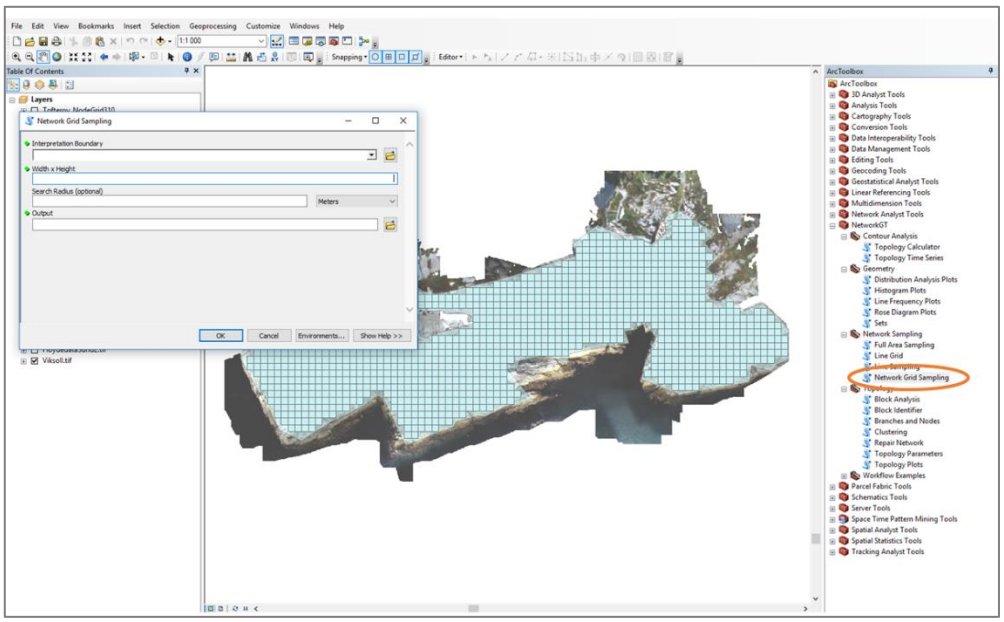


6. Branches and nodes for each cell could then be extracted using the '**Branches and nodes'** tool, using the fracture network polylines, grid sample area and interpretation

area as inputs. When the branches and nodes are extracted, the different topological parameters can be calculated by the **'Topology Parameters'** tool, which create a duplicate polygon feature class of the network grid with information about the topological parameters.

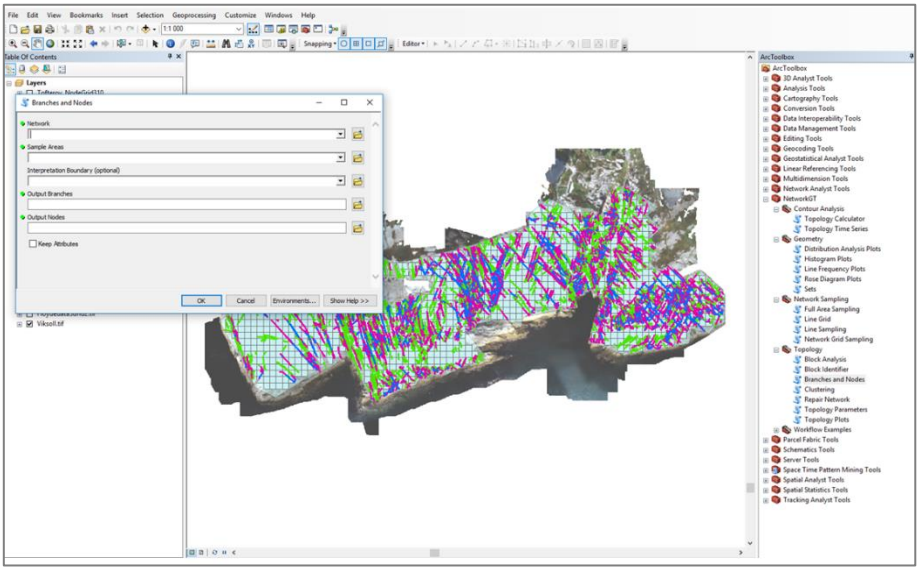

7. To assess the spatial variability of the topological parameters, quantities and graduated colours where chosen in the Properties box under symbology. Here different parameters to assess can be selected.

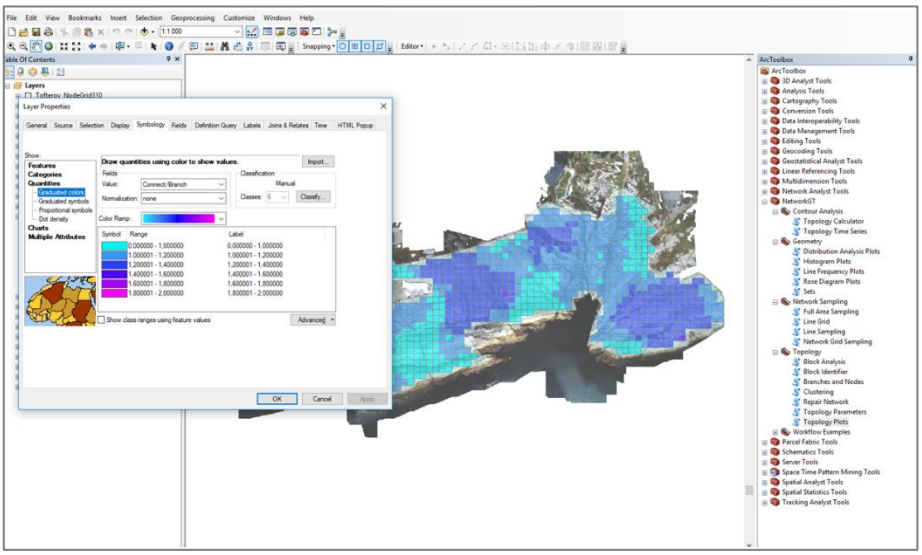

# Appendix II – Raw data linear scanlines

Raw data from linear scanlines in separate attachment.